ASM Handbook, Volume 7: Powder Metal Technologies and Applications
P.W. Lee, Y. Trudel, R. Iacocca, R.M. German, B.L. Ferguson, W.B. Eisen, K. Moyer,
D. Madan, and H. Sanderow, editors, p 840-858
DOI: 10.1361/asmhba0001577

Advanced Aluminum Powder Metallurgy Alloys and Composites

Ram B. Bhagat, The Pennsylvania State University

POWDER METALLURGICAL PROCESSING provides much finer and homogeneous microstructure, better mechanical properties, and near-net shape parts producibility for aluminum alloys in comparison with ingot metallurgy (I/M). In addition to the conventional blending and consolidation of elemental or prealloyed powders into near-net shape parts, emerging processes such as mechanical alloying and rapid solidification (RS) create composite powders that upon subsequent consolidation provide significant improvements in room and elevated-temperature strength, fracture toughness, fatigue life, and corrosion resistance. The real advantage of P/M processing including spray forming is in the production of new alloys and composites with metallurgical structures and compositions that cannot be produced by I/M. Rapid solidification extends the solubility of alloying elements, particularly transition and rare earth elements, and refines the structure of intermetallic phases responsible for improved mechanical properties. Mechanical alloying is a dry, high-energy milling process producing dispersions of insoluble oxides and carbides that stabilize the microstructure leading to high strength at elevated temperatures in the consolidated materials. By blending the alloy powder with a strengthening phase, discontinuously reinforced aluminum-matrix composites containing insoluble dispersoids (oxides and carbides), particulates, whiskers, or fibers are produced for high-performance structural applications (Ref 1–6). Table 1 includes the chemical composition of aluminum P/M alloys and dispersion-strengthened composites.

Aluminum-matrix composites with reinforcement of particulates, whiskers, or chopped fibers have been widely studied worldwide. They are generally isotropic and less costly in comparison with continuous-fiber-reinforced aluminum-matrix composites. The discontinuously reinforced aluminum (DRA) composites are attractive for near-term commercial applications. Silicon carbide (SiC) or alumina-particle-reinforced aluminum composites have higher stiffness and, in general, high wear resistance in comparison with the unreinforced aluminum alloys. Silicon carbide whisker, however, is currently the most widely utilized reinforcement for the DRA composites for obtaining high resistance to creep and higher use temperatures. Early work on whisker reinforcement started in the 1960s. Brenner (Ref 7, 8) and Sutton (Ref 9, 10) used α-Al_2O_3 whiskers to fabricate metal-matrix composites (MMCs). These early composites were not attractive because of their relatively low strength and the high cost of the whisker. Later Divecha et al. (Ref 11) used SiC whiskers to fabricate aluminum-matrix composites with good mechanical properties. In 1973, Cutler (Ref 12) introduced his patented process of inexpensively producing SiC whiskers from pyrolized rice hulls. This renewed the interest in the development of whisker-reinforced MMCs (Ref 13–16). There have been concerns in handling fine particulates and whiskers because of health risks. For pathogenic reasons such as mesothelioma induction and fibrogenic and lung cancer potential, it has been found that it is the size and shape of any given particle that causes problems, as well as its chemistry (Ref 17, 18). Hence it is advisable to use particulate with diameters greater than 5 μm and to avoid contact with fibers or whiskers in the range 0.1 to 3 μm, with lengths greater than 5 μm. There has been only a limited interest in whiskers other than SiC for fabricating MMCs. Recently Imai, Nishida, and Tozawa (Ref 19) evaluated the mechanical properties of aluminum-matrix composites with Si_3N_4 whisker. The composites, fabricated by P/M hot pressing and subsequently extruded, showed good mechanical properties. Limited work has been reported on continuous-fiber-reinforced aluminum composites fabricated by P/M processing. Bhagat and coworkers (Ref 20–25) fabricated stainless steel wire (type 304) reinforced aluminum-matrix composites by hot pressing (800 K, 155 MPa, and 60 s). The composites showed attractive mechanical properties including high fracture toughness and fatigue life. These composites are suitable for structural applications requiring high fracture toughness and high resistance to impact damage.

Selection of suitable composition of the matrix material is important to meet mechanical and physical property requirements of the aluminum-matrix composites. Minor alloying additions in the wrought alloys are generally detrimental to the mechanical properties of the composites because of undesirable interfacial reaction (Ref 26–28) during the P/M consolidation. The P/M route for producing the discontinuously reinforced composites involves blending elemental or prealloyed powder with the reinforcement, followed by canning, vacuum degassing, and some form of consolidation, such as hot pressing or hot isostatic pressing (HIP), into a billet that is subsequently rolled, forged, or extruded into shapes. During the billet consolidation, however, the matrix alloy may experience incipient melting, creating both large insoluble and excess soluble intermetallics, which form upon resolidification of aluminum alloy matrix. These particles are deleterious to the fracture toughness and ductility of the DRA. This has led to the recent development of the leaner variants of the 2*xxx* and 6*xxx* series aluminum alloys (e.g., 2009 and 6090), which contain strengthening elements in concentrations no greater than their mutual solubilities, thereby leading to useful ductility and fracture toughness in the composites (Ref 29–31). It is important to note, therefore, that the compositional and microstructural requirements are different for dispersion-strengthened alloys and particle or whisker-reinforced aluminum composites.

In addition to fabricating shaped structures, deformation processing (extrusion, forging, or rolling) of the consolidated composites develops the best properties attainable by breaking up any preexisting oxide on the alloyed powder. Extrusion of whisker-reinforced composites leads to an approximate alignment of the whiskers in the extrusion direction. Production of useful shapes requires, at least to some extent, secondary processing such as machining and joining, which are not well established for the composites. Conventional machining of composites is very difficult because of the high hardness of the ceramic reinforcement. Expensive diamond or cubic boron

nitride cutting tools are needed for effective machining. The high-cost conventional machining of MMCs can be eliminated by near-net shape manufacturing or by noncontact machining techniques such as laser processing (Ref 32) and abrasive waterjet cutting (Ref 33). Large-scale commercialization of the aluminum P/M alloys and composites is still small (compared to wrought and cast aluminum alloys), although new applications are emerging (see "Applications Outlook" in this article). Notwithstanding the high cost that remains a major concern for their use, there are other major technological challenges such as reproducibility/reliability, machining, joining, and recycling that need to be addressed.

Table 1 Chemical composition of aluminum P/M alloys including dispersion-strengthened composites

Alloy designation	Composition
Al-C	Al-3.0C
Dispal 2	Al-2.0C-1.0O
Al-Cu-C	Al-1.0Ci-1.5C
Al-Mg-C	Al-2.0Mg-1.5C
Al-Cr-X	Al-5.0Cr-2.0Zr-1.0Mn
Al-Ti-X	Al-3.0Ti-3.0Ce
Al-Be-X	Al-22.6Be-10.8Li
201AB	Al-4.4Cu-0.8Ci-0.5Mg-1.5 other
201AC	Al-4.4Cu-0.8Si-0.5Mg
202AB	Al-4.0Cu-1.5other
601AB	Al-0.25Cu-0.6Si-1.0Mg-1.5 other
601AC	Al-0.25Cu-0.6Si-1.0Mg
602AB	Al-0.6Mg-0.4Si-1.5 other
MD-76	Al-5.6Zn-2.5Mg-1.6Cu
7090	Al-8.0Zn-2.5Mg-1.0Cu-1.5Co-0.35O
7091	Al-6.5Zn-2.5Mg-1.5Cu-0.4Co
X7090	Al-0.12Si-0.15Fe-(0.6–1.3)Cu-(2–3)Mg-(7.3–7)Zn-(1.0–1.9)Co
X7091	Al-0.12Si-0.15Fe-(1.1–1.8)Cu-(1–3)Mg-(5.8–7.1)Zn-(0.2–0.6)Co
X7093	Al-9.0Zn-2.2Mg-1.5Cu-0.14Zr-0.10Ni
8009	Al-8.5Fe-2.4Si-1.3V
X8019	Al-8.3Fe-4.0Ce
Al-Fe-Ce	Al-8.0Fe-3.5Ce-0.35O
Al-Fe-Co	Al-(3–8)Fe-(2–7)Co-0.35O
Al-Fe-Ni	Al-8Fe-1.7Ni
Al-Fe-Mo	Al-8.0Fe-2.0Mo
Al-Fe-Ni-Co	Al-5Fe-3Ni-6Co
Al-Fe-Cr	Al-8.5Fe-1.5Cr-0.35O
XAP001	Al-0.2Fe-0.40C-0.08Si-6.0 oxide
XAP002	Al-0.28Fe-0.19C-0.10Si-8.0 oxide
XAP004	Al-0.29Fe-0.39C-0.10Si-14.0 oxide
IN9021	Al-4.0Cu-1.5Mg-1.2C-0.75O
IN9051	Al-4.0Mg-0.7C-1.4O
IN9052	Al-4.0Mg-0.75O-1.0C
905XL	Al-4.0Mg-1.3Li-0.4O-1.1C
Al-Li-Cu	Al-(2–3.5)Cu-0.5Mg-0.6Mn-(2.5–3.2)Li
Al-Mn-Co	Al-(3–8)Mn-(1.5–7)Ni
Al-Mn-Ni	Al-(3–8)Mn-(1.6–6.5)Co
Al-Ni-Co	Al-(2–5)Ni-(2–5)Co

Source: Ref 1–3

Conventional Consolidation

For wrought aluminum P/M alloys such as 601AB and 201AB (see Table 1), prealloyed aluminum powders are cold isostatically pressed into green compacts, degassed, and sintered in nitrogen atmosphere; sintering in dissociated ammonia or vacuum leads to relatively inferior mechanical properties. The cold compaction, degassing and sintering are done typically at 400 MPa, 450 °C, and 600 °C, respectively (Ref 1). The as-sintered products are usually not fully dense and have relatively low strengths. They require heat treatment and deformation processing (rolling, extrusion, or forging) for improved properties (see Table 2).

For full densification, powder particles are compacted isostatically and encapsulated in an aluminum canister. The compact is heated, and gases are evacuated from the canister. The heated canister/compact is pressed into a billet with 100% density. The canister is removed from the billet by machining. The billet is subsequently fabricated into parts by rolling, forging, or extrusion. The conventional P/M processing of the aluminum-matrix composites include the following steps. The reinforcement particulates/whiskers (see Table 3) are deagglomerated prior to mixing or blending in a suitable medium. Ultrasonic agitation of whiskers or fine particulates suspended in alcohol or wet milling in a polar solvent medium such as *n*-butanol is required to eliminate the problem of agglomeration. The deagglomerated mass is mixed with matrix alloy powder and subjected to a dry or wet blending process to obtain a uniform distribution of the reinforcement in the matrix. Improper blending leads to an inhomogeneous distribution of the reinforcement in the final product. The solvent is removed by drying the powder mixture in air. As an example, the powder mixture of 2124 Al and SiC particulates can be heated at 150 °C to remove *n*-butanol from the blend (Ref 34). The mixture is cold compacted in a die using a hydraulic press. Carbowax and stearic acid are suitable lubricants for the die wall to prevent wear. Level of densification is critical to provide some green strength for handling and yet leave behind an open interconnecting pore structure so as not to hinder degassing. Both the physically absorbed and chemically combined water on the matrix alloy powder particles are liberated in the form of water vapor during the degassing. If the degassing is incomplete, the postcompaction thermal exposure can give rise to hydrogen evolution due to reaction between the water vapor and aluminum. This causes blistering in the billet and reduces ductility and fracture toughness of the composite. Degassing temperature and time are critical parameters because lower times and temperatures lead to incomplete degassing, whereas higher times and temperatures lead to a chemical reaction between the matrix and the reinforcement that can result in a weak interface. Jain et al. (Ref 34) experimentally determined the optimal temperature and time of 723 K and 1 h, respectively, for degassing of the 2124/SiC_p green compact. Vacuum hot pressing or HIP is required for final consolidation of the degassed green compact. Full densification is obtained by optimizing the temperature, pressure, and the period of hot pressing. Further details on the conventional P/M processing of particulate or whisker-reinforced metal composites can be found elsewhere (Ref 34–44).

Table 2 Mechanical properties of nitrogen-sintered wrought aluminum alloys

Alloy	Yield strength, MPa	Ultimate tensile strength, MPa	Elongation, %
201AB-T6 (95% dense)	322	336	2
201AB-T6 (97% dense, rolled)	327	332	2
202AB-T6 (92.4% dense)	147	227	7.3
202AB-T8 (92.4% dense, cold formed, 19% strain)	250	280	3
601AB-T6(96% dense)	230	238	2
601AB-T6 (96% dense, rolled)	241	252	2
602AB-T6 (96% dense)	172	186	3

Source: Ref 1

Table 3 Typical properties of particulate, whisker, and discontinuous fiber reinforcements

Property	SiC_p	Al_2O_{3p}	TiB_{2p}	Si_3N_{4p}	Al_2O_3 (Saffil)	SiC_w	Si_3N_{4w}	$K_2O{\cdot}6TiO_{2w}$
Density, g/cm^3	3.21	3.97	4.5	3.18	3.3	3.19	3.18	3.3
Diameter, μm	...	...	...	...	3–4	0.1–1.0	...	...
Thermal expansion coefficient, 10^{-6}/K	4.3–5.6	7.2–8.6	8.1	3.0	~9	4.8	3.8	...
Tensile strength, MPa	100–800(a)	70–1000(a)	700–1000(a)	250–1000(a)	>2000	3,000–14,000	13,800	6,900
Young's modulus, GPa	200–480	380	514–574	304	300	400–700	379	274
Elongation, %	...	...	...	...	0.67	1.23	...	...
Composition	...	...	...	...	96%-Al_2O_3-4% SiO_2	>98% SiC	...	...

(a) Transverse rupture strength of bulk

Emerging Technologies

The primary advantage of P/M processing, as mentioned before, is due to the use of emerging technologies such as mechanical alloying, rapid solidification, and spray forming, which provide a greater flexibility in tailoring the composition and microstructure of dispersion-strengthened aluminum alloys and composites with or without particulate/whisker reinforcement.

Mechanical Alloying and Processing (MAP). Mechanical alloying is used for fabricating oxide-dispersion-strengthened alloys and discontinuously reinforced composites. Pure metal powder and alloying ingredients are mechanically alloyed using high-energy ball mills. During this process, a heavy working of powder particles results in the intimate alloying by a process of repeated welding, fracturing, and rewelding (Ref 45–56). In the case of aluminum alloys, carbon derived from process control agents and incorporated into the processed powder reacts with aluminum to form very fine carbides. These carbides and the fine oxide particles derived from the breakup of surface films on the initial powder particles create a dispersion that stabilizes the fine-grained microstructure. Therefore, a portion or all of the strengthening may be obtained from the ultrafine grain size stabilized by the oxide and carbide dispersions (see Ref 4). Mechanically alloyed (MA) product (i.e., the composite powder) is subsequently consolidated into suitable shapes. The mechanical alloying is also useful in developing materials with large contents of alloying additions for improving mechanical properties at elevated temperatures. This processing technique alleviates the problems of low solubility according to the phase diagram or possibility of forming low-melting equilibrium or nonequilibrium phases. Thus, an anomalous supersaturation can be achieved in systems such as aluminum-iron, aluminum-nickel, aluminum-chromium, and aluminum-titanium by mechanical alloying with or without particulate additions. Such materials have potential for improved strength at elevated temperatures. A novel use of the mechanical alloying is in the generation of amorphous alloys that, upon subsequent controlled crystallization, can generate nanometer-scale microstructures (Ref 57–59). The MA aluminum powder 9052 shows improved mechanical properties and corrosion resistance. MA Al-12.5Ti alloy has a stable, ultrafine grain structure containing fine Al_3Ti particles of 20 to 250 nm in size. This alloy has high stiffness, good ductility, and high strength at elevated temperatures. Bhaduri et al. (Ref 60) used mechanical alloying to prepare composite powders of 7010 Al from elemental powder with or without SiC particulates. The addition of SiC particulates appears to inhibit the progress of mechanical alloying. The composites had higher modulus but lower strength values than the matrix at room temperature. However, at temperatures >200 °C the composites exhibited higher tensile strength than the matrix. Other examples of MAP aluminum alloys and composites and their properties are discussed later.

Rapid Solidification and Processing (RSP). Rapid solidification is a "far-from-equilibrium" process that results in a significant undercooling of the molten metals or alloys leading to a refinement of microstructural features and constitutional effects such as extension of solubility limits, synthesis of novel crystalline phases, and formation of metallic glasses (Ref 3, 61–66). Fabrication of particle-reinforced MMCs by the RSP involves introduction of the particulates into the melt, proper mixing, melt spinning, and canning of the composite particles, followed by extrusion or forging or both into finished shapes. Rapid solidification processing has enabled the development of a new family of high-strength aluminum alloys for elevated-temperature applications. The RSP alloys such as those based on hypereutectic aluminum-iron compositions derive their high strengths from dispersion strengthening; the dispersoids resist dissolution and coarsening when the alloys are exposed to elevated temperatures. Aluminum 7091 and 7090 are Al-Zn-Mg-Cu alloys that are similar in composition to I/M 7175, but contain 0.4 and 1.45% Co, respectively. Cobalt forms Co_2Al_9 or $(Co,Fe)_2Al_9$ particles that are homogeneously dispersed. These dispersoids refine the grain size for improved high strength and ductility and enhance the resistance to stress-corrosion cracking (Ref 3). Kumpfert et al. (Ref 67) produced high-silicon-content (~20 wt%) aluminum alloys with high strength at room to elevated temperatures by combining RSP and the mechanical alloying. Courtreight et al. (Ref 68) used RSP for fabricating SiC-particle-reinforced aluminum composites with significantly improved mechanical properties.

A number of aluminum-base amorphous alloys have been fabricated by melt spinning (Ref 69–73). These aluminum glasses (with or without the presence of aluminum nanocrystals) show very high tensile strength and low density. The rapidly solidified and processed $Al_{70}Ni_{20}Zr_{10}$, $Al_{90}Fe_5Ce_5$, and $Al_{89}Ni_7Y_4$ metallic glasses with 25 vol% of nanocrystals can have yield stresses up to 1550 MPa, good ductility, and high elastic modulii (Ref 3, 74–76). Generally, these amorphous alloys have poor thermal stability. The problem of poor thermal stability can, however, be alleviated by compositional optimization as reported by Jin et al. (Ref 69). They found that iron in the range of 35 at.% in the rapidly solidified $Al_{86}Mm_4Ni_{1-x}Fe_x$ (at.%) alloys (Mm represents mischmetal, 49Ce-25La-18Nd-5.4Pr-2.6 other, wt%), provides optimal compositions having good thermal stability combined with high strength for practical structural applications.

Spray forming is a high-deposition-rate metal spraying process for the production of near-net shape parts at a relatively low cost. In this method, molten metal is rapidly atomized to form a fine spray of droplets that are deposited onto a stationary or moving collector. This forming process has proven to be a viable and cost-effective alternative to conventional metalworking technology for the production of metal preforms with properties superior to I/M. Spray forming has been demonstrated to create new materials such as new compositions of aluminum alloys (Ref 77–80), MMCs (Ref 81–87), and those suitable for semisolid forming (Ref 88). The spray-formed products are typically free from macrosegregation and prior-particle boundaries that are occasionally present in the conventional P/M products. The spray forming is useful in extending the maximum solute content of alloying elements and achieving a finer distribution of second-phase particles in an equiaxed fine-grain structure. Such homogeneous, low-segregation, fine-scale alloy microstructures are useful for subsequent rolling, forging, extrusion, and superplastic forming operations. The development of low-density aluminum-lithium alloys has a high potential for significant weight savings in aerospace structures. Alloys produced by conventional casting methods are currently limited to lithium levels of approximately 2.5 wt%. Above this level, it is difficult to avoid the formation of coarse second-phase particles and achieve low levels of hydrogen and alkali metal impurities in the cast ingots. Hydrogen and sodium are known to have an embrittling effect in aluminum-lithium alloys. A high hydrogen level also has detrimental effects on the weldability. These concerns can be eliminated by the spray-forming process that offers a number of significant advantages for producing aluminum-lithium alloys:

- Increasing solute content
- Refining of microstructure
- Elimination of oxide films
- Reduction of hydrogen and sodium levels

Examples of spray-formed aluminum-lithium alloys are UL30 and UL40 having increased levels of lithium and zirconium in comparison with one of the most commonly used aluminum-lithium alloys, 8090 (Al-2.5Li-1.0Cu-0.7Mg-0.12Zr). According to White et al. (Ref 89), UL30 (Al-3.0Li-1.0Cu-0.7Mg-0.3Zr) shows a 4.4% increase in specific modulus over 8090, and the strengthening is primarily by duplex particles of fine Al_3Zr (β') and Al_3Li (δ') and copper and magnesium in solid solution. These duplex particles form without the need of cold working, unlike 8090 in which stretching is required to enhance precipitation of the σ' (Al_2LiMg) phase. Thus, tensile properties of unstretched UL30 can equal those of stretched 8090, with improved isotropy. By obviating the need for cold work, UL30 can be fabricated in near-net shapes by the spray forming process. Palmer et al. (Ref 78) have spray formed UL40 (Al-4Li-0.2Zr) with lithium content reaching the limit of solid solubility at the eutectic temperature. They found the as-sprayed grain structure equiaxed with grain sizes in the range 40 to 50 μm. They also found the presence of some relatively coarse δ phase (AlLi) at the grain boundaries and some needlelike δ phase in the grains. The amount of this fine δ phase was greatest at the spray-form cen-

ter and decreased toward the surface, indicating that this phase precipitated as a result of slow cooling in the solid state. As expected, no coarse Al_3Zr particles were observed in the microstructure due to a relatively high solidification rate suppressing their formation. A small amount (<1%) of porosity was present in the as-sprayed materials, which disappeared during subsequent extrusion. The extrusion grain structure was very fine and highly elongated. Some of the intergranular δ phase was present in the microstructures. However, most of the intergranular δ phase and all of the intragranular needlelike δ phase were dissolved upon subsequent solution heat treatment.

Based on the transient heat transfer during droplet solidification via finite element analysis (Ref 90), Bhagat (Ref 91) developed a model for solidification and growth kinetics of the primary silicon in spray-formed (Osprey) Al-17Si alloy (Fig. 1). The predicted results were found to agree with the experimental results. Buhrmaster et al. (Ref 92) fabricated SiC-particle- or whisker-reinforced aluminum composites by spray casting. In this process, aluminum wire feedstock is melted and combined with SiC particulates or whiskers entrained in an inert gas. Upon striking a substrate or mold, the mixture of aluminum and SiC solidifies into a composite structure. The fabricated composites lacked uniform distribution of the reinforcement. Discontinuously reinforced MMCs were fabricated by a spray codeposition method wherein the reinforcement particulates or whiskers were introduced into the metal spray leading to their codeposition with the atomized metal onto the substrate (Ref 93, 94). Typical recovery efficiency of the spray codeposition method is 60 to 90%, depending on the product form such as hollow tube, forging stock, extrusion ingot, or plate. Precise control of gas pressures and particulate feed rates are required to ensure that a uniform distribution of particulate is produced within the matrix that may be 95 to 98% dense. The shape of the final product depends on the atomizing conditions and the shape and motion of the collector. Willis

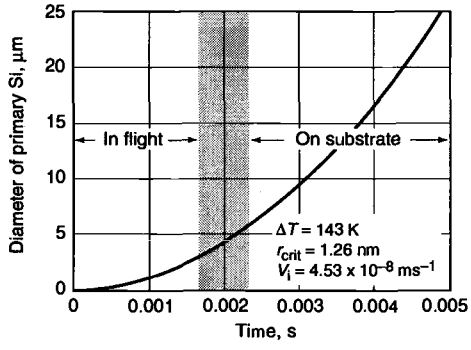

Fig. 1 Predicted size of primary silicon in an spray-formed (Osprey) Al-17Si alloy during in-flight cooling and subsequent cooling on the substrate. The prediction is based on a new and validated model for grain growth kinetics developed by the author. ΔT, r_{crit}, and V_i represent undercooling, critical radius of silicon, and instantaneous growth rate, respectively.

(Ref 93) reported uniform distribution of the particulates in a 2014/SiC/15_p composite (15 vol% SiC particulates) fabricated by the spray codeposition method. The average particle diameter was approximately 13 μm; the starting material was F600 SiC grit. Willis (Ref 93) also reported spray codeposition of aluminum-lithium 8090 reinforced with SiC particulates. The composites were subsequently extruded into shapes. The overall strength of the fabricated 8090/SiC_p composites in the peak aged condition did not show much improvement over the matrix material. However, the improvement in specific modulus for 8090/SiC_p (density = 2.62 g/cm^3) over the unreinforced aluminum alloy (density = 2.55 g/cm^3) is almost 50%. One of the primary reasons for the attractive properties of the spray-formed MMCs is the integrity of the particle/matrix interface. The interface is free from any precipitate or reaction product in Al/SiC composites according to Warner et al. (Ref 95) as reported in Ref 94. This is attributed to the relatively small (a few seconds) contact time between molten metal and SiC in the spray codeposition. Wu and Lavernia (Ref 96) fabricated 6061Al/SiC_p composites by spray-atomized codeposition technique. A maximum of 16% increase in stiffness of the composite over that of the unreinforced matrix was achieved. Other mechanical properties of the spray-formed composites are discussed later in this article.

In another variation of the spray-forming technology, Siemers et al. (Ref 97) used a low-pressure plasma deposition (LPPD) method for producing MMCs. In this process, a plasma (~10,000 to 20,000 K) is formed in the interior of a gun (commonly referred to as plasma gun) by the discharge of a high-intensity dc arc through a flowing gas mixture (argon or N_2 with additions of 2 to 15% H_2 or helium). Powder is injected into the plasma jet through one or more injector ports. The powder is then entrained in the high-velocity (Mach 2 to 3) plasma jet, melted, transported, and impacted on a substrate where the molten droplets solidify at cooling rates of 10^5 to 10^6 K/s. The LPPD process can be used for most metals, metal carbides, or metal oxides excluding those materials that decompose before melting. Siemers et al. (Ref 97) produced composites of metal-metal, metal-carbide, and metal-oxide combinations. They also produced graded layered structures of near-theoretical density to minimize the effects of interfacial stresses developed due to the thermal mismatch between the constituents. Both continuous and discontinuous composite laminates can be fabricated by the LPPD process. Continuous laminates, consisting of alternating layers of metal and reinforcement, are produced by first depositing metal, subsequently depositing the reinforcement, and repeating the sequence to build the desired final thickness. The proportions of the phases and the layer thickness can be varied over considerable ranges to produce tailored composites. For fabricating discontinuous laminates consisting of individual splattered particle lamellae (2 to 4 μm thick and 50 to 150 μm diameter), a powder blend of two or more different compositions can be injected into the plasma jet.

Other Technologies. In addition to the aforementioned emerging technologies, there are other P/M processing techniques such as XD process, solid free-form fabrication (SFF), and self-propagating high-temperature synthesis (SHS), which also show potential for developing high-performance aluminum alloys and composites including functionally graded materials. In the proprietary XD process (Martin Marietta, Baltimore, MD), elemental components of the desired reinforcing phase are mixed with or incorporated into the metallic matrix material. The mixture is heated to a high temperature (>T_m) where a self-propagating reaction takes place. The elemental constituents react exothermally, forming a dispersion of submicroscopic reinforcing particles in the matrix. Because the particles of the reinforcing phase are formed by an exothermic reaction at an elevated temperature, they tend to be very stable through subsequent processing and use at high temperatures. However, if both elemental constituents of the particulate phase have high diffusivity in the matrix phase, then particle coarsening may occur at high temperatures. In addition, particle shape may change during heat treatment or use at elevated temperatures, if the surface energies are different. Christodoulou et al. (Ref 98) and Larsen et al. (Ref 99) used the XD process to produce a master-alloy material containing TiB_2 particles (TBA-70 sponge: 70 wt% TiB_2 and 30 wt% Al), which was subsequently used for fabricating the discontinuously reinforced aluminum composites.

Solid free-form fabrication facilitates integrated manufacturing, from computer-aided design (CAD) to finished parts, using only additive processing (Ref 100, 101). A solid or surface model is electronically sectioned into layers of predetermined thickness. The sections collectively define the shape of the part. Information about each section is then transmitted layer by layer to the SFF machine. Material is consolidated only at solid areas of the section. Subsequent layers are sequentially processed until the part is complete. It is this sequential, layered, or lithographic approach to parts manufacturing that defines the SFF technology. Selective laser sintering (SLS) and the selective laser reactive sintering (SLRS) are examples of the SFF technology for producing MMCs. Net-shape composite components can be directly produced from the elemental or prealloyed matrix powders mixed with suitable reinforcement by sintering, layer by layer, under a scanning laser beam; the reinforcement phase may be formed in situ.

Self-propagating high-temperature synthesis is a process in which the synthesis reaction proceeds through the reactant mixture in the form of a combustion wave (Ref 102–106). The progression of the wave is driven by the energetics of the reaction and the characteristics of the reactants. Some of the advantages of the SHS processing may include purity of the product, energy efficiency, formation of metastable phases, and

simultaneous synthesis and densification. The SHS process thus has the potential to be a viable method for producing high-performance MMCs.

Functionally graded materials (FGMs) including MMCs create a continuous transition from an essentially ceramic material exposed to high temperatures to a partly or fully metallic material at the lower-temperature side of the structure (Ref 107–112). Such graded structures have been created in an AlN/Al composite using the conventional P/M technology (Ref 108, 113).

Table 4 Properties of P/M aluminum alloys and composites

Reinforcement contents are reported in vol%, if not otherwise specified. The composition of MMCs is described using a nomenclature system developed by the Aluminum Association.

Material	0.2% yield strength, MPa	Ultimate tensile strength, MPa	Elongation, %	Young's modulus, GPa	Reference
1100/SiC/10_p extruded	75	114	20	96	115
2009/SiC20_p-T8					
Longitudinal	462	593	5.2	109	116
Transverse	421	572	5.3	109	116
2014/SiC/20_p	466	493	2	100	2, 117
2014 Al	429	476	7.5	72	10
Alloy 201 (Al-4.4Cu-0.5Mg-0.8Si, wt%); aged 160 °C, 14 h	300	335	1.1	...	118
201/SiC(23 μm)/9_p	295	310	0.3	...	118
201/SiC(63 μm)/9_p	285	290	0.3	...	118
201/SiC(142 μm)/9_p	260	265	0.3	...	118
2080/SiC/15_p K_{Ic} = 33 MPa$\sqrt{m}$	365	483	7	100	2, 117
2080/SiC/20_p K_{Ic} = 22 MPa$\sqrt{m}$	393	517	6	110	117
2124/SiC/18_p solution treated					
At 485 °C	409	610	8.6(a)	...	114
At 545 °C	453	679	9.4(a)	...	114
At 585 °C	373	577	7.8(a)	...	114
2124/SiC/25_p-T6	496	738	5.0	117	31
6013/SiC/15_p-T6	434	517	6.3	101	116
6013/SiC/20_p-T6	448	538	5.6	110	116
6013/SiC/25_p-T6	469	565	4.3	121	116
6061 Al	330–347	365–386	13.6–14.4	70	29
6061/SiC/20_p	373	389–409	1.0–1.3	89	29
6061/Al_2O_3/20_p	317	354–361	3.6–4.1	95	29
6061/SiC/10_p/Al_2O_3/10_p	357	391	1.6	94	29
6061 Al	89	171	25.0	...	
At 473 K	85	127	29.3	...	32
At 723 K	20	23	46.2	...	32
6061/SiC/20_p (5μm)	123	224	7.3	...	32
At 473 K	119	163	16.7	...	32
At 723 K	23	25	20.1	...	32
6090/SiC/25_p-T6	393	483	5.5	117	31
6090/SiC/40_p-T6	427	538	2.0	138	31
7001/SiC/25_p-T6	655	724	1.5	117	31
7049/SiC/15_p	598	643	3	90	117
7075/SiC (5μm)/11_p K_Q = 15.7 MPa$\sqrt{m}$	570	630	6.6	...	119
7075/SiC (13 μm)/17_p K_Q = 13.6 MPa$\sqrt{m}$	595	645	3.5	...	119
7075/SiC (60 μm)/17_p K_Q = 18.5 MPa$\sqrt{m}$	501	504	0.6(a)	...	119
7075/SiC/15_p	556	601	4	95	117
7090 K_{Ic} = 31 MPa$\sqrt{m}$	579	621	9	74	2
7091 K_{Ic} = 46 MPa$\sqrt{m}$	545	593	11	72	2
X7093 K_{Ic} = 47 MPa$\sqrt{m}$	579	614	12	75	2
7475/SiC/25_p-T6	593	655	2.5	117	31
8009 K_{Ic} = 11 MPa$\sqrt{m}$	605	636	9	...	2
Monolithic 8009					
At 25 °C	407	448	17	88	30
At 149 °C	345	365	9	...	30
At 232 °C	296	310	11	...	30
At 371 °C	165	186	19	...	30
8009/SiC/11_p					
At 25 °C	496	544	5.5	102	
At 149 °C	400	427	3.5	...	
At 232 °C	310	338	4.2	...	
At 371 °C	193	220	7.0	...	
X8019	338	427	5	79	2
8090/SiC/15_p K_{Ic} = 14 MPa$\sqrt{m}$	499	547	3	101	117
8090/SiC/17_p-T6 designated as A817	...	542	4–6(a)	103	120
8090/SiC/18_p-T6	531	621	3.2	103	31
9052 K_{Ic} = 44 MPa $\sqrt{m}$	380	450	13	76	2
905 XL K_{Ic} = 30 MPa $\sqrt{m}$	450	520	9	...	2
Dispal 2	340	380	12	80	2
Al-Fe-Mo	393	512	10	82	2
Al-Cr-X	426	460	14	86	2
Al-Ti-X	255	294	22	...	2
Al-Be-X	483	510	20	96	2
Al-12Si (forged)	298	336	2.5	80	121
Al-25Si-AlN (reaction sintered)	...	350	...	80	122
Al-4Ni-2Fe-AlN (reaction sintered)	...	350	...	80	122
Al-7Si-20SiC-AlN (reaction sintered)	...	300	...	90	122

(a) Strain to failure

Mechanical Properties

The discontinuously reinforced aluminum composites, as mentioned earlier, are extruded, forged, or rolled to develop the best properties attainable by breaking up the prior-particle oxide skins. Usually a homogenization annealing is needed to dissolve the intermetallic inclusions in the matrix formed during vacuum hot pressing or HIP. Thomas and King (Ref 114) established an optimal solution treatment (545 °C, 6 h, 33 min) for an extruded P/M 2124/SiC/18_p composite for improved mechanical properties (see Table 4). In the DRA composites, the difference between the coefficients of thermal expansion (CTE) of the matrix aluminum alloys and the reinforcement is very significant. Compare the CTE of pure aluminum, which is 24×10^{-6}/K with those in Table 3 for particulate and whisker reinforcements. The CTE mismatch leads to a high dislocation density at interfaces, thereby creating complex residual stresses in the composite, putting matrix in tension and the reinforcement in compression, during the cooling from the processing temperature. The residual stresses adversely affect the mechanical behavior and dimensional stability of the composites. Li et al. (Ref 123) eliminated the residual stresses in P/M 6061/SiC/20_p by low-temperature treatments between –60 °C (ethanol + liquid nitrogen) and –196 °C (liquid nitrogen) and subsequent reheating to room temperature.

Fracture

The strengthening mechanisms and fracture of the dispersion-strengthened aluminum alloys are well understood (see Ref 4). However, the same is not true for the particulate- or whisker-reinforced aluminum composites exhibiting a complex frac-ture behavior. Silicon carbide particle-reinforced aluminum composites are of particular interest for stiffness critical applications. They possess high shear strength in comparison with matrix materials (see Table 5). The tensile properties of these composites, however, cannot be easily predicted. Mechanical properties included in Table 4 suggest that even similar materials have large differences in yield strength and ultimate tensile strength. The ductility, in general, is significantly lower than the matrix alloys. Wang et al. (Ref 118) developed a method to quantify particle cracking behavior as a function of strain in Al/SiC/9_p (23, 63, or 142 μm SiC particulates) composites fabricated by liquid-phase sintering. The particle crack area and the frequency of cracked particulates were found approxima-tely linear as a function of local strain along the direction of the tensile loading. The particle crack area at a given strain was not significantly affected by reinforcing particle

size, but did increase with increasing matrix strength. The frequency of cracked particulates was affected by both reinforcing particle size and matrix strength. The particulates in the composites with high matrix strength are more highly stressed and, therefore, are more likely to fracture. Consider, for example, the mechanical properties of 2124/SiC_p in Fig. 2 reported by Jain et al. (Ref 34) and those in Table 4 by Harrigan (Ref 31). Jain et al. (Ref 34) extruded 2124/SiC_p at 773 K at a ram speed of 33 mm/s for an extrusion ratio of 16 to1 in the direct extrusion mode. The tensile strength initially increases with increase in the reinforcement volume fraction, peaks at 20 vol%, and then decreases (see Fig. 2). The maximum tensile strength obtained by Jain et al. is only about 50% of that reported by Harrigan for comparable small specimens. Similarly, the yield strength and the ductility are substantially lower for the composites fabricated by Jain et al. in comparison with that of Harrigan. Similar comparisons can be made for other systems. Table 4 includes the mechanical properties of heat treated 7075/SiC/11_p and 7075/SiC/17_p composites (Ref 119). In high-strength aluminum alloys such as 7000 series the reinforcement led to a decrease in yield stress and tensile strength, relative to the matrix alloy, together with reduced ductility. Doel et al. (Ref 119) discuss the fracture micromechanisms to explain the observed high toughness values for low ductility composites (see Table 4). It becomes clear that the choice of matrix compositions, reinforcement particle size, fabrication procedures, and even the test procedures play important roles in reconciling and reproducing desired level of mechanical properties.

Mechanical properties of the whisker-reinforced aluminum-matrix composites are included in Table 6. The whisker-SiC/Al composites (SiC_w/Al) have high specific strength and stiffness (Ref 41, 43, 128–131) as well as resistance to creep deformation (Ref 131). Komai et al. (Ref 127) found that apart from the elongation at failure, the mechanical properties of the 7075/SiC/20_w-T6 composite were superior to those of an unreinforced 7075-T6 alloy. There has been only a limited interest in whiskers other than SiC for fabricating MMCs. Recently Imai, Nishida, and Tozawa (Ref 19) evaluated the mechanical properties of extruded P/M aluminum-matrix composites with Si_3N_4 or $K_2O{\cdot}6TiO_2$ whiskers. The properties of these whiskers are included in Table 3. Elastic modulus of the composites is about 1.6 times that of the matrix. Tensile strength of the 6061/Si_3N_4/25_w composite is 560 MPa, which is comparable to that of

Table 5 Shear strength of SiC-particulate-reinforced aluminum composites

Composite	Shear strength, MPa
6061 Al (T-6)	207
25 vol% SiC/6061 Al (T-6)	277.9
30 vol% SiC/6061 Al (T-6)	289.6
7075 Al (T-6)	269
25 vol% SiC/7091 Al (T-6)	379.2
30 vol% SiC/7090 Al (T-6)	430.9
2124 Al (T-4, T-6)	283
2124 Al (T-81)	295
25 vol% SiC/2124 Al (T-4)	344.8

Source: Ref 37

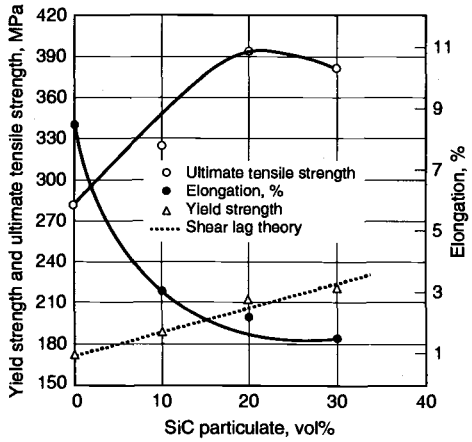

Fig. 2 Mechanical properties of SiC particle-reinforced 2124 Al composites (vacuum hot pressed and extruded). Source: Ref 34

Table 6 Properties of whisker-reinforced aluminum-matrix composites

The composition of MMCs is described using a nomenclature system developed by the Aluminum Association. Reinforcement contents are reported in vol%, if not otherwise specified.

Material	0.2% yield strength, MPa	Ultimate tensile strength, MPa	Elongation, %	Young's modulus, GPa	Reference
2009/SiC/15_w-T8					
Longitudinal	483	634	6.4	106	116
Transverse	400	552	8.4	98	116
2124/SiC/20_w (wt%) K_{Ic} = 18.7 MPa$\sqrt{m}$	377	527	2.2(a)	110	124
2124-T8 K_{Ic} = 31 MPa$\sqrt{m}$	440	490	8(a)	...	125
6013/SiC/15_w-T6	469	655	3.2	119	116
6061-T6	225	290	17	70	126
6061/SiC/20_w	...	630	2.0	...	44
6061 SiC/20_w	440	585	4	120	126
6061 SiC/30_w	570	795	2	140	126
6061/Si_3N_4/25_w	...	560	...	...	19
7075/SiC/20_w	740	844	1.6	122	127

(a) Strain to failure

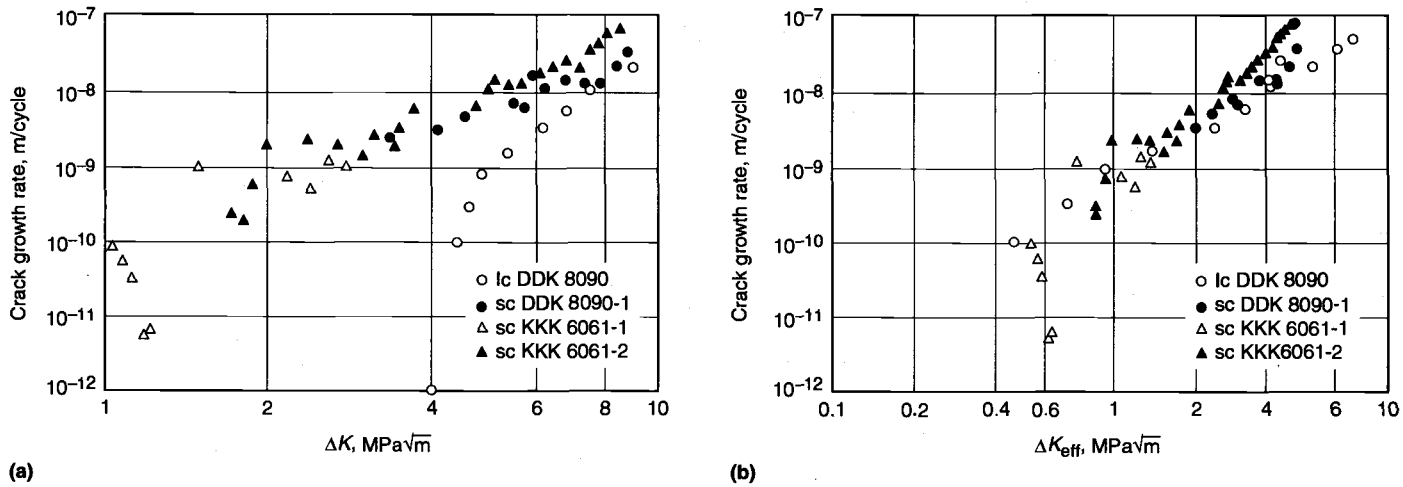

Fig. 3 The growth of large (lc) and small (sc) fatigue cracks compared on the basis of $\Delta K_{applied}$ (a) and ΔK_{eff} where closure effects have been removed (b). All data are from Ref 144 and 145 as reported in Ref 143.

the SiC whisker-reinforced aluminum composites (Table 6). The ultimate tensile strength of $K_2O{\cdot}6TiO_2$ /Al is about 200 MPa at 573 K. Mechanical properties of the MAP and RSP aluminum alloys and composites are presented in Table 7. Table 8 includes the mechanical properties of the spray-formed aluminum alloys and composites.

Fatigue

A number of crack-tip shielding mechanisms including crack closure via asperity wedging in a coarse-particle-reinforced composite and crack bridging via uncracked ligaments in a composite reinforced with fine particulates have been identified during fatigue crack growth (Ref 141). The fatigue crack growth behavior in an Al/SiC/20_p composite having a strong interface has been examined by Shang and Liu (Ref 142). They suggest that the fatigue crack growth in the composite can be characterized as particle controlled. The interaction of the crack-tip stress field with the particulates results in microcracking, development of uncracked ligaments behind the crack tip, and local trapping of the crack front. Recently, Davidson (Ref 143) reviewed the mechanisms and fracture mechanics of fatigue crack initiation and the growth of small and large fatigue cracks and fracture toughness in aluminum alloys reinforced with SiC and alumina particulates. Fatigue cracks initiate within clumps of and at broken reinforcement particulates, and at intermetallic particles in the matrix. Small fatigue cracks grow faster than would be anticipated from the growth of large cracks and at lower stress-intensity range (ΔK). When ΔK for small and large cracks is adjusted for plasticity-induced fatigue crack closure to give ΔK_{eff}, the growth of all sizes of fatigue cracks are comparable (see Fig. 3). The source of fracture toughness in these composites is homogeneous crack-tip plasticity; fracture occurs at limiting values of strain or work dissipation within the crack-tip deformation zone. This is consistent with the results (see Fig. 4) reported by Doel et al. (Ref 119), who studied the mechanical properties of aluminum-base particulate MMCs fabricated by cospray deposition process (Ref 147). They found that as the particle size is increased from 13 to 60 μm, for a nominally constant volume fraction and for a given aging condition, the uniaxial tensile ductility falls, but the toughness increases.

Cernyar et al. (Ref 124) studied the fatigue of SiC whisker-reinforced aluminum composite under load control at 10 Hz, load ratios being 0.1 and 0.5. The composite exhibited a lower plane strain fracture toughness value than the matrix material, but a significantly higher resistance to fatigue crack growth in comparison with the wrought 2124 Al. For the composite, they obtained Paris law exponent n as 5.4, which is higher than that of the matrix (3 to 4), and a threshold stress intensity of 5.5 MPa$\sqrt{m}$ under a stress ratio R of 0.1. The complex fatigue damage mechanisms included whisker bridging, whisker pullout, crack deflection along the whisker/matrix interface, whisker tip voids, and whisker fracture. Komai et al. (Ref 127) investigated the fatigue behavior of 7075/SiC/20_w-T6. They found that a fatigue crack initiated at a whisker cluster or a crack at the specimen surface. They also found that the fatigue strength of the composite at a stress ratio of 0.1 was higher than that of an unreinforced 7075-T6 alloy. Narasimhan et al. (Ref 148) evaluated a P/M 6061/SiC/20_w composite for its thermomechanical fatigue performance at temperatures of 150 and 300 °C at a stress ratio of 0.1 under stress-controlled testing. They compared the high-temperature fatigue performance of the composite in terms of a stress-strain product plotted against cycles to fracture. The use of the stress-strain product term alleviates the problem of often reaching conflicting conclusions based on the conventional S-N type plots for strain-controlled and stress-controlled tests on composites.

Wear

The dispersion-strengthened aluminum alloys and composites generally have the potential for enhanced wear resistance over the matrix alloy (Ref 148–152). Murakami (Ref 3) has reported improved wear resistance of RSP Al-20Si-2Cu-

Table 7 Properties of MAP and RSP aluminum alloys and composites

The composition of MMCs is descried using a nomenclature system developed by the Aluminum Association. Reinforcement contents are reported in vol%, if not otherwise specified.

Material	0.2% yield strength, MPa	Ultimate tensile strength, MPa	Elongation, %	Young's modulus, GPa	Reference
MAP AA2014 (extruded)					
As extruded	...	450	...	...	132
-T6	...	563	...	...	132
MAP 7010/SiC/15_p (wt%)	...	182 at 573 K	...	...	133
MAP 7010					
At room temperature	412	498	1.85(a)	74.2	60
At 150 °C	...	377	...	...	60
At 150 °C	...	138	...	...	60
At 150 °C	...	80	...	...	60
MAP 7010Al	...	275 85 at 573 K	0.68(a)	79.7	134
At 150 °C	...	331	...	...	134
At 150 °C	...	176	...	...	134
At 150 °C	...	93	...	...	134
MAP 7010/SiC/20_p (wt%)					
At room temperature	394	414	0.59(a)	93.5	60
At 150 °C	...	313	...	...	60
At 150 °C	...	184	...	...	60
At 150 °C	...	131	...	...	60
RSP 7090	595	637	10	...	3
RSP X7090-T6E192 (extruded)	641	676	10	73.8	1
RSP X7091-T6E192 (extruded)	558	614	11	72.4	1
RSP AA8009	401	450	19	...	135
MAP					
AA8090 (extruded)	...	475.8	3.78	78.6	136
AA8090/SiC/8.2_p	...	488.5	2.45	88.3	136
AA8090/SiC/10_p	...	494.6	1.92	92.4	136
AA8090/SiC/15_p	...	519.3	1.25	104.5	136
MAP 9052Al K_{Ic} = 44 MPa$\sqrt{m}$	380	450	13	76	3
MAP Al-12.5Ti	...	...	...	104	3
At 220 °C	...	220	...	...	3
At 450 °C	...	150	...	...	3
RSP Al-10Fe-5Ce	357	453	8	...	136
RSP FVS1212 (Al-8.5Fe-1.3V-1.7Si)	522	572	23	...	135
RSP Al-8Fe-2.3Mo	460	510	7	...	135
RSP Al-25Si (extruded)	...	500	...	95	122
MAP Al-Li-Mg-O-C K_{Ic} = 45 MPa$\sqrt{m}$	450	510	10	...	137
Al-Li + 20wt% SiC_p	...	542	...	...	138
RS-MAP Al-12Si-5Mn-2Ti + 8 wt% SiC	450 360 at 423 K 240 at 573 K	...	...	...	67
RSP A356/SiC/15_p (10–15 μm)	296	358	6.1	93	68

(a) Strain to failure

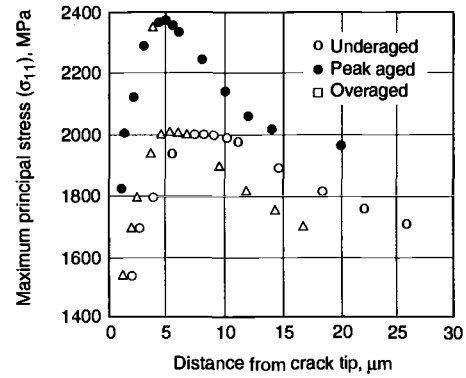

Fig. 4 Local maximum principal stress distributions in SiC-particle (5 μm) reinforced aluminum composites ahead of the crack tip, just prior to failure. From Ref 19 and 146 as reported in Ref 143

1Mg alloy. Jin et al. (Ref 151) evaluated the wear performance of RSP Al-8.5Fe-1.3V-1.7Si-Ti and Al-16Si-5Fe-3.5Cu-1.2Mg-SiC_p against steel (65 HRC) over a range of sliding speed (0.16 to 1.26 m/s) under a load of 42 N at ambient and 150 °C under dry conditions. For both the materials, the wear rate first decreased with increase in sliding speed, reached a minimum and then increased at higher sliding speed. The transition sliding speed appeared to change the wear mechanism from abrasive wear (at low speed) to wear accompanying plastic deformation (at higher speed). Pin-on-disk wear tests on AA6061 composites containing Saffil, SiC_p, or mixtures of both ceramics against SiC grit and steel counterfaces, showed that composites containing only Saffil had inferior wear resistance to those containing the same volume fraction of SiC_p (Ref 149). Bialo and Duszczyk (Ref 152) studied the wear of Al_2O_3/Al composite fabricated by liquid-phase sintering using a pin-on-disk apparatus for pressure (p) and sliding speed (v) range of 0.3 to 3 MPa and 0.1 to 5 m/s, respectively. They observed that the "pv" product is the most significant factor describing the wear process; stable friction and wear behavior of the material occurs only for pv below a threshold value of 3 MPa · m/s. They also observed that the reinforcement particle size has less significant effect on the wear rate than the pv product. Wang and Rack (Ref 153) have reported good wear resistance of SiC_w/Al. Dry sliding wear of DRA composites has been reviewed by Sannino and Rack (Ref 150). In general, DRAs offer substantially better wear resistance than the matrix alloy. However, under particular conditions and wear mechanisms, the wear performance of the overall DRA-metal couple is similar to or lower than the matrix alloy-metal couple. Furthermore, conflicting results regarding the effect of the different tribological parameters on the wear performance of DRAs are observed. This is primarily attributed to interactions of wear parameters; these interactions are currently not well understood.

High-Temperature Performance

The dispersion-strengthened aluminum alloys and composites are most attractive for their high-temperature strengths. Particulate or whisker reinforcement enhances their high-temperature capabilities further. Zedalis et al. (Ref 30), for example, developed high-temperature discontinuously reinforced aluminum composites for elevated-temperature applications by incorporating SiC particulate into a rapidly solidified, high-temperature Al-Fe-V-Si (alloy 8009) matrix. On a specific stiffness basis, this composite is competitive with Ti-6Al-4V and 17-4 PH stainless steel to temperatures approaching 753 K (see Fig. 5). In this section, the high-temperature performance of aluminum P/M alloys and composites are discussed in terms of their aging effects on tensile strength and toughness, strength at elevated temperatures, and creep.

Aging Effects

The aging characteristics of spray-atomized and codeposited 6061Al/SiC_p composites are discussed by Wu and Lavernia (Ref 96). There was no evidence of any interfacial reaction products in the composites. They found an enhancement of the interfacial bond strength due to the interdiffusion of the alloying elements into the reinforcing particulates, upon heat treatment. Downes and King (Ref 154) evaluated the fracture behavior and fracture toughness of 8090/SiC/20_p (wt%) as a function of matrix aging condition. The composite was produced by BP Metal Composites (Farnborough, UK) using a P/M route involving HIP, hot forging, and finally hot rolling to a plate thickness of 15 mm. They found the toughness values almost independent of reinforcement size (3, 6, and 23 μm). Aging at 443 K resulted in a monotonic decrease in toughness with increasing strength up to the peak condition, with no subsequent recovery in toughness on overaging.

Bhagat and coworkers (Ref 155–159) investigated the aging characteristics of SiC-whisker-reinforced 6061 Al composites ($V_f = 0.20$) received from Advanced Composite Materials Corporation (Greer, SC) in the form of 11.4 by 10.2 by 3.8 cm slabs. The composite was fabricated by a proprietary P/M method followed by extrusion in order to align the whiskers and increase tensile strength in the extrusion direction. The whiskers were found approximately aligned in the direction of extrusion as described in Ref 156. Both tensile dog-bone specimens and hardness samples were heat treated. These samples were placed into steel packets to protect against surface oxidation throughout the entire heat treatment process. The hot-worked condition of the as-received material was removed by first solutionizing the composite. A ramping period of 3 h (2.78 K/min) was used to obtain a stable solutionizing temperature of 803 ± 5 K. This temperature was held for 15 min, and then the samples were immediately water quenched. The

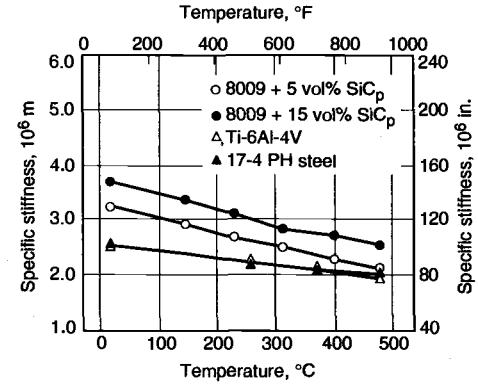

Fig. 5 Elevated-temperature specific stiffness of high-temperature discontinuously reinforced aluminum composites compared to that of titanium and stainless steel, reported in Ref 30

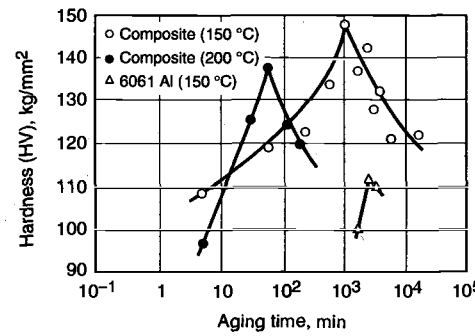

Fig. 6 Aging response of 6061/SiC/20_w and wrought 6061 Al. The composite shows accelerated aging response.

Table 8 Properties of spray-formed aluminum alloys and composites

The composition of MMCs is described using a nomenclature system developed by the Aluminum Association. Reinforcement contents are reported in vol%, if not otherwise specified.

Material	0.2% yield strength, MPa	Ultimate tensile straight, MPa	Elongation, %	Young's modulus, GPa	Reference
2014 Al	429	476	7.5	72	93
2014/SiC/10_p spray codeposited, extruded, peak aged	457	508	1.8	81.2	94
2014/SiC/15_p spray codeposited, extruded, peak aged	...	...	...	95	93
2014/SiC/20_p	466	493	2	100	2, 117
2080/SiC/20_p, K_{Ic} = 22 MPa$\sqrt{m}$	393	517	6	110	2, 117
2618Al spray codeposited, rolled, peak aged	345	400	7	72	94
2618/SiC_p spray codeposited, rolled, peak aged	396	468	3.3	93.6	94
6061 Al spray codeposited, extruded, peak aged	224	266	18.3	65.5	94
6061/SiC/13_p spray codeposited, extruded, peak aged	317	356	4.9	89.5	94
6061/SiC/11.5_p-T6 spray atomized and codeposited	293	330	8.2	79.7	96
6061/SiC/14_p-T6 spray atomized and codeposited	294	330	9.0	...	139
6061/SiC/28_p-T6 spray atomized and codeposited	322	362	5.0	...	139
7049/SiC/15_p	598	643	3	90	2, 117
7075/SiC/15_p	556	601	4	95	2, 117
8090Al	480	550	5	79.5	93
8090/SiC_p spray codeposited, extruded, peak aged	486	529	2.6	100	93
8090/SiC/15_p, K_{Ic} = 14 MPa$\sqrt{m}$	499	547	3	101	2, 117
Al-20Si-5Fe-2Ni					
Air atomized (Osprey), sintered at 550 °C, 1 h	...	346	0.78(a)	...	140
Nitrogen-atomized (Osprey), sintered at 550 °C, 1 h	...	360	0.82(a)	...	140

(a) Strain to failure

solutionized samples were aged for periods of 5 min to 3 h at 473 K and for periods of 5 min to 500 h at 423 K. Following the aging, microhardness was measured at a load of 800 g using the Vickers hardness scale. Twenty values of microhardness were used to obtain the average hardness of the composite under various aging conditions.

Figure 6 includes the measured microhardness of SiC_w/6061 Al aged at 423 and 473 K. The peak microhardness value is 137.7 kg/mm^2 at 473 K, while at 423 K the peak microhardness value is 147.9 kg/mm^2. Peak aging times were 60 min and 18 h for aging temperatures of 473 K and 423 K, respectively. As a comparison, the peak microhardness for the resolutionized wrought 6061 Al is 111.7 kg/mm^2. Figure 6 demonstrates that the composite has significantly higher microhardness than the wrought 6061 Al. The high microhardness of the composite is attributed to the cumulative effect of the matrix material and whisker reinforcement. However, the trend of the aging response of the composite is primarily dependent on the aging response of the matrix. As the matrix hardens, the hardness of the composite increases until the peak is reached, followed by a drop in hardness due to the overaged matrix. The plots in Fig. 6 demonstrate the accelerated aging response of the composite as compared to the wrought 6061 Al. At the aging temperature of 423 K, peak hardness of the composite is achieved 25 h earlier, and it is 20% higher than the peak hardness of 6061 Al. For the composite, the lower aging temperature of 423 K causes the peak value of hardness to be 7% greater and 17 h later with respect to the higher aging temperature of 473 K. It is well known that the composite has a large dislocation density because of the thermal mismatch between matrix and fiber (Ref 160, 161). The high dislocation density speeds up the nucleation and growth of precipitates leading to the rapid precipitation hardening of the matrix in the composite (Ref 162). Such an accelerated aging for DRAs is also reported by other investigators (Ref 153, 163, 164).

The stiffness of the solutionized and aged composite remains constant around 105.68 GPa (as shown in Fig. 7), which is 28% lower than that of the as-received extruded composite having a stiffness of 147.55 GPa. Stiffness values of the aged composite are of practical significance for high-temperature applications, and they are about 53% higher than that of the wrought 6061-T6 Al. The tensile strength of SiC_w/6061 Al was measured as a function of aging time. Results in Fig. 8 show that the strength of the composite reaches a maximum value in the peak-aged condition. This shows that the dislocation entanglement and the finely dispersed precipitates lend maximum strength at the peak hardness. A 27% decrease in tensile strength is seen from the as-received condition. This is due to the solutionizing step that eliminated the prior hardening or strengthening due to the extrusion of the composite. Plots in Fig. 8 provide further evidence of the accelerated aging of the composite as discussed earlier. Maximum strength in the composite is reached 37 h earlier than 6061 Al with an increase of 40% in strength when measured from peak to peak. Maximum strength in the composite is maintained from 18 to 55 h; whereas 6061 Al peaks in strength at 55 h. Despite the overaging of the matrix (18 to 55 h), the strength of the composite remains almost constant. Aging the composite for 500 h reduces the ultimate tensile strength from 516 to 398 MPa, which still results in an increase of 27% over that of the identically aged wrought aluminum alloy. Ductility of the aged composite was found substantially higher than that of the as-received material which had a maximum elongation of 2%. Strain to failure was obtained by the strain versus load plot up to the fracture load. The

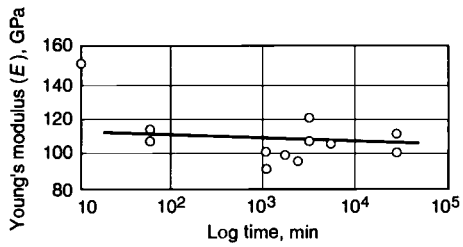

Fig. 7 Young's modulus versus aging time for solutionized 6061/SiC/20$_w$ aged at 423 K. After an initial drop, the Young's modulus is not much affected by the aging time.

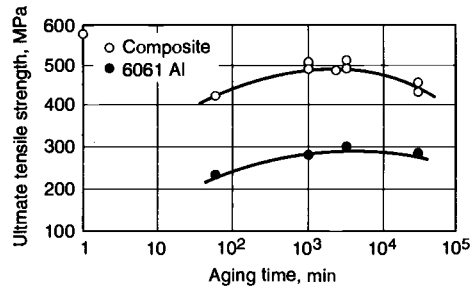

Fig. 8 Room-temperature tensile strength of solutionized 6061/SiC/20$_w$ and resolutionized 6061 Al aged at 423 K

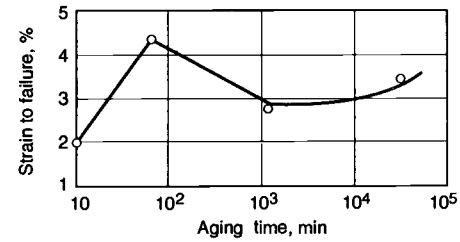

Fig. 9 Elongation to failure for solutionized 6061/SiC/20$_w$ aged at 423 K

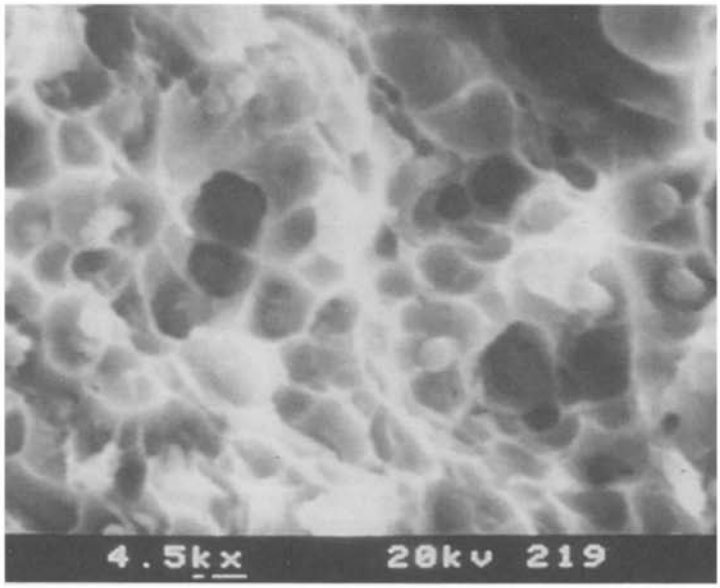

Fig. 10 SEM fractograph of 6061/SiC/20$_w$ aged for 18 h at 423 K (peak aged conditions)

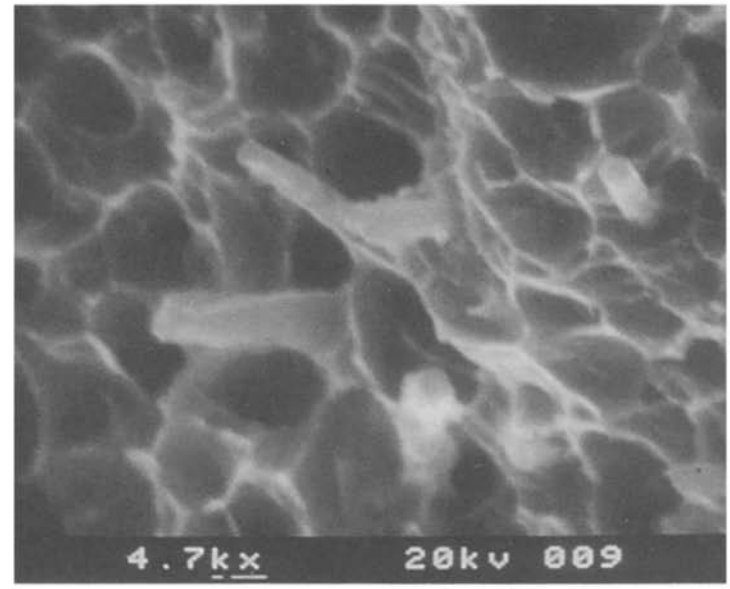

Fig. 11 Whisker pullout in 6061/SiC/20$_w$ aged for 500 h at 423 K

composite shows minimum strain to failure in the as-received condition (Fig. 9). The general trend of the elongation—rapid increase in ductility upon solutionization and aging, then decreasing, reaching a low value, and then gradually increasing with the aging time—is as expected. The work of fracture for the composite material is maximized in the overaged condition (500 h at 150 °C) having a value of 8.07 MJ/m^3 compared to the as-received condition, which has a work of fracture of 0.35 MJ/m^3. Ductile fracture as a result of microvoid coalescence can be seen in the tensile test fracture surface shown in Fig. 10. The fractograph represents a peak-aged composite showing that the whiskers serve as the initiation sites for microvoids. Nutt (Ref 165) has studied and modeled void nucleation at the whisker ends in SiC_w aluminum composites. He found through transmission electron microscopy (TEM) analysis that the voids initially formed at the corners of the whiskers. Figure 11 shows a pulled-out whisker relatively free of interfacial reaction products.

Strength at Elevated Temperatures

Bhagat and coworkers (Ref 155–158) studied the elevated temperature mechanical properties of discontinuously reinforced aluminum-matrix composites. The unsolutionized SiC_w/6061 composite and wrought 6061-T6 Al specimens were subjected to elevated-temperature tensile testing over the range of 423 to 623 K. High-temperature strain gages were mounted to accurately determine Young's modulus and the ultimate tensile strength. Testing temperature was maintained within ±3 K of the desired set point. A uniform temperature distribution was achieved in the composite specimen by soaking at the testing temperature for 20 min prior to loading. Figures 12 and 13 depict the results of test temperatures on stiffness and ultimate tensile strength, respectively. Stiffness for the composite remains almost constant in the temperature range of 423 to 623 K, while strength decreases gradually. In the as-received condition, the composite exhibits a 111% improvement over 6061 Al in stiffness. At elevated temperatures, the stiffness of the composite exhibits a 56% improvement as compared to wrought 6061 Al. Comparing the ultimate tensile strength of the composite and 6061 Al, the whisker reinforcement at room temperature gives 114% improvement over 6061 Al, decreasing to only a 60% advantage at 623 K. The strength of the composite at elevated temperatures becomes matrix dominated as it is expected for discontinuously reinforced MMCs. An SEM fractograph showing ductile fracture because of microvoid coalescence is given in Fig. 14 for SiC_w/Al tested at 561 K. It can be seen in Fig. 14 that the whiskers form initiation sites for microvoids.

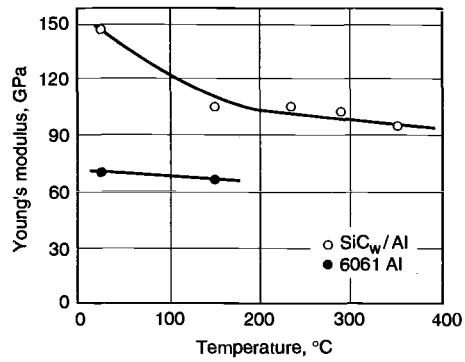

Fig. 12 High-temperature stiffness of 6061/SiC/20_w and wrought 6061 Al

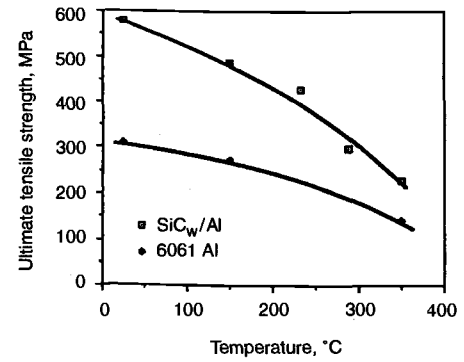

Fig. 13 High-temperature ultimate tensile strength of unsolutionized 6061/SiC/20_w and wrought 6061-T6 Al

Creep

Several researchers have studied the creep behavior of aluminum-base alloys and composites (Ref 131, 157, 158, 166–183). The deformation mechanisms for creep of metals and alloys include:

- Dislocation glide due to slip
- Dislocation climb leading to subgrain formation
- Sliding of grain boundaries
- Diffusion of vacancies

These mechanisms may be related to creep deformations of the matrix in the composite, but the influence of the reinforcement is not well understood. The dispersion-strengthened alloys and reinforced composites, generally, show a change of stress exponent from a low to a relatively high value (see Table 9). The creep strength of these high-temperature aluminum alloys is significantly higher than the conventional wrought aluminum alloys. In addition, the creep resistance for the whisker-reinforced aluminum composites has been shown to increase with increasing volume fractions of the reinforcement (Ref 181). Their improved creep resistance can be attributed to the effective load transfer from the matrix to the whiskers and the inhibition of dislocation motion by the whiskers. Bhagat and coworkers (Ref 157, 158) performed the creep testing of 6061/SiC/20_w composite on an 88.96 kN capacity Arcweld creep rupture machine. This machine is equipped with an automatic horizontal leveling arm and a three-zone Arcweld furnace. The temperature of the furnace was monitored with thermocouples located within the furnace and located next to the gage length. Displacements were measured by an LVDT attached to stainless steel grips. The creep tests were conducted over a temperature range of 505 to 623 K and for applied stresses of 60 to 200 MPa. The steady-state creep rates ($\dot{\varepsilon}_{ss}$) for the MMCs as a function of stress (σ) and temperature (T) are represented by the power-law creep equation, which has been historically used for the unreinforced matrix alloys:

$$\dot{\varepsilon}_{ss} = A\sigma^n \exp(-Q_a/RT) \quad \text{(Eq 1)}$$

The stress exponent (n), activation energy (Q_a) and the constant A of the creep power law (Eq 1) are important parameters in creep studies. The steady-state creep involves steady deformation at high temperatures and stresses. Bhagat et al. (Ref 158) experimentally determined that for an applied stress under 100 MPa, a well-behaved second-stage creep rate existed for the 6061/SiC/20_w composite. The activation energy of the composite was determined by an isostress plot of the natural log of $\dot{\varepsilon}_{ss}$ and $1/T$ as shown in

Table 9 Steady-state creep results for P/M aluminum alloys and composites

Material	Volume fraction(a), %	Dispersoid size, nm	Grain size, μm	Stress exponent	Activation energy, kJ/mol	Reference
Al-Ti	8	54	0.5	7–8	240	168
Al-Fe-Ni	19–32	100	0.3	9.0–12.9	310–329	169
Al-Fe-Ni	19–32	100–160	0.2–0.3	9.6–12.9	...	170
Al-Fe-Ce	22	...	0.5	0.8–8.7	61–172	171
Al-Fe-Ce	25	...	0.5	1–8	84–142	172
Al-Fe-V-Si	36	30–80	<0.5	13–32	360	173
Al-Fe-V-Si-Er	27	87	0.4	14.7	342	174
Al-Cr-Zr	25	400	1.0	1.0	82	175
Al-Zr-V	5	30	0.5	14	...	176
Al-Zr-V	5–15	...	0.4–0.9	1	84	177
Al-Fe-W-Si	25–36	80	0.3	1.5–16	...	178
6061/SiC/20_w	...	...	...	...	390	131
6061/SiC/20_w (solutionized)	...	...	...	20	390	179
6061/SiC/20_w (unsolutionized)	...	...	...	16	76	158
2124/SiC/20_w	...	...	...	...	277 at 149–204 °C	180
					431 at 274–302 °C	180
Wrought 6061	...	...	...	3	...	179

(a) Volume fraction of dispersoids

Fig. 15. A comparison of the activation energy value obtained by Bhagat et al. (Ref 158) is made in Table 9 with the published results of other investigators. Differences between the values of the activation energy can be attributed to the solution treatment of the samples prior to the creep testing. Bhagat et al. (Ref 158) determined the stress exponent (n) of 16, representing the slope of the plot shown in Fig. 16. Figure 16 also shows a much smaller value of n in the low-stress regime, which can be ignored considering the high-strength capabilities of the composites. The high-stress regime n of 16 signifies that the composite is more stress sensitive compared to the wrought aluminum. This is true because the stress concentrations are developed at the whisker ends wherein the damage is initiated (see Fig. 17). The fractograph in Fig. 17 represents a creep-rupture surface of the composite tested at 561 K under a load of 100 MPa; the expected dimple morphology is noticeable. The steady-state creep rates for the whisker-reinforced composite, included in Table 10, clearly demonstrate that the composite has improved resistance to creep in comparison to the wrought 6061 Al.

Deformation Processing

Secondary processing such as rolling, forging, or extrusion in conjunction with suitable heat treatment is required to develop desired physical and mechanical properties of the aluminum alloys and the DRA composites in addition to producing useful shaped structures (Ref 35, 37, 115, 184). The formability of DRAs, however, is greatly restricted by the incompatible deformation characteristics of the soft matrix and the hard reinforcement. The optimal processing parameters for the matrix materials generally do not apply to the reinforced composites.

Rolling, Forging, and Extrusion

Near-net shape components of DRAs are produced by closed-die forging methods developed for high-strength aluminum alloys. Large components are forged directly from billet using a series of blocker and finish dies. Small parts can often be forged from extruded stock in fewer processing steps. Sheet and plate are hot rolled on conventional rolling mills from extruded bar or extruded-and-forged plate. Most P/M billets are extruded to rods or rectangular bars using lubricated conical or streamline dies. Rods can be reextruded into a variety of shapes using conventional shear-face dies. It has been reported that the forged aluminum parts have strength 40 to 60% higher than nonforged parts (Ref 1). Fatigue endurance limit is double that of nonforged P/M parts. Alloys 601AB, 602AB, 201AB, and 202AB are designed for forging. All of the aluminum P/M alloys respond to strain hardening and precipitation hardening, providing a wide range of properties. Properties of cold-formed P/M alloys are increased by a combination of strain-hardening densification and improved interparticle bonding.

Jokinen and Wiik (Ref 185) studied high temperature formability and mechanical properties of aluminum-matrix composites. They suggested that bulk forming operations applying large compressive forces (extrusion or die forging) are to be preferred when forming the composites. Bhat et al. (Ref 115) studied the constitutive flow behavior of 1100/SiC/10_p under hot-working conditions to generate a processing map. They suggested that the composites be extruded in the dynamic recrystallization regime at a temperature of 500 °C, wherein the dynamic recrystallization reconstitutes the microstructure and redistributes the prior-particle-boundary defects for improved formability. Cernyar et al. (Ref 124) rolled 2124/SiC/20_w into plate for improved properties. Various structural shapes, in addition to round and rectangular tubing, have been produced from composites containing up to 25 vol% SiC_w (Ref 116).

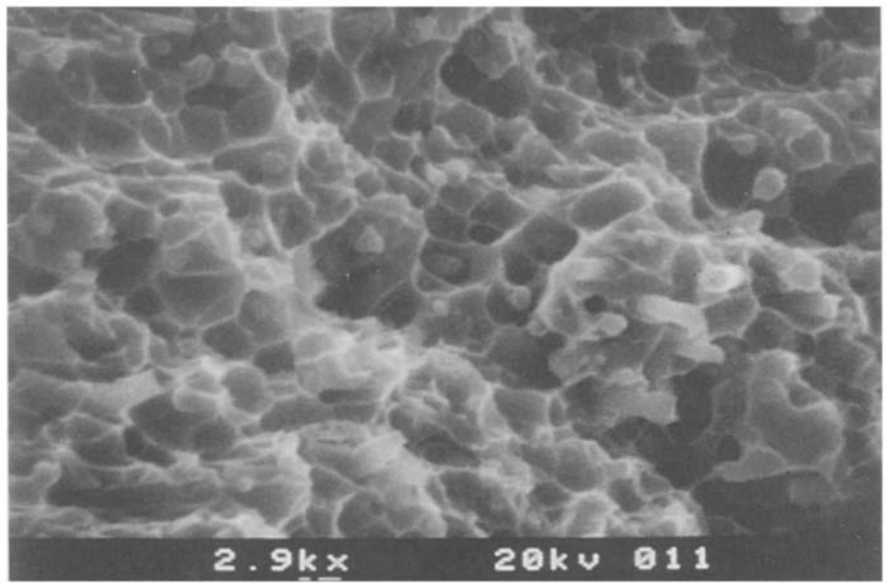

Fig. 14 SEM fractograph of unsolutionized 6061/SiC/20_w tensile tested at 561 K

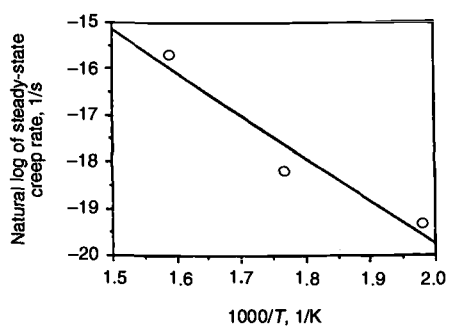

Fig. 15 Steady-state creep rate of SiC-whisker-reinforced 6061 Al composite at three temperatures. The slope of the plot is used for calculating the activation energy of the composite.

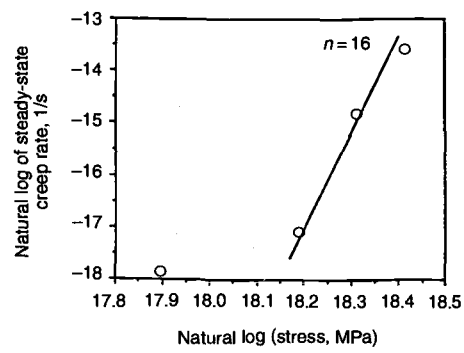

Fig. 16 Logarithmic steady-state strain rate versus logarithmic stress plot. The slope of the plot defines the stress exponent.

Superplastic Forming

Superplasticity is the ability of polycrystalline material to exhibit, in a generally isotropic manner, very high tensile elongation prior to failure. The high-strain-rate superplasticity (HSRS) is of great interest because it is expected to result in economically viable, near-net shape forming techniques for practical applications. Several P/M aluminum alloys and composites exhibit superplastic behavior at high strain rates over 10^{-2} s^{-1} (Ref 186–188). Figure 18 shows that the high-strain-rate superplasticity is associated with a very small grain size (<3 μm). It signifies that a fine grain size is a necessary condition for superplasticity, but it is not a sufficient condition for the observed HSRS phenomenon. Tensile elon-

Table 10 Steady-state creep rates for wrought 6061 Al and a P/M 6061/SiC/20_w composite

Temperature, °C	Stress, MPa	Steady-state creep rate, s^{-1}
Composite		
232	58.7	4.901×10^{-9}
293	59.1	1.287×10^{-8}
293	79.6	3.890×10^{-8}
298	89.6	3.758×10^{-7}
293	99.3	1.278×10^{-6}
356	60.0	1.546×10^{-7}
Wrought 6061 Al, 288	60.0	5.000×10^{-6}

gations of 1250 and 1400% have been achieved in the MAP IN9021 and 6061/SiC/20$_w$, respectively (see Table 11). Figure 19 shows that the mechanically alloyed IN9021 and IN9021/SiC/15$_p$ exhibit superplastic deformation. Mabuchi and Imai (Ref 189, 190) have reported fabrication of Si_3N_4-reinforced 2124 or 6061 Al composite having superplasticity. The 8090/SiC/17$_p$ composite in conjunction with superplastic forming has been used for fabricating net-shape components such as a module door for aircraft (Ref 120). Grain-boundary sliding is the principal deformation mechanism during the HSRS flow. The accommodation processes that must take place to allow continued grain boundary sliding include:

- Partial melting at grain boundaries
- Melting at interface
- Adiabatic heating as a result of large strain deformation at high strain rates
- Dynamic recrystallization
- Grain-boundary diffusion
- Lattice diffusion

These accommodation processes, however, are not well understood.

Technological Challenges

In spite of significant advances in developing high-performance aluminum P/M alloys and composites, there remain major technological challenges that include reproducibility and reliability of performance, machining, joining, and recycling for making these materials attractive and affordable for large-scale commercial applications.

Reproducibility

Process models can be used to simulate the consolidation process, predict stress states and relative density distribution during and after processing, design special tools, and design processing schedules to ensure reproducibility, thus avoiding high cost of trial-and-error-based experiments (Ref 191, 192). For example, the mechanisms that contribute to densification of powder materials during HIP include plastic yielding, power-law creep, and lattice and boundary diffusion. Ashby and coworkers (Ref 193–196) have developed models for each densification mechanism, in each stage of densification, for the case of pure hydrostatic stress. These mechanisms are greatly influenced by the presence of ceramic particulates or whisker reinforcements. Even in the absence of any reinforcement, nonhydrostatic stress fields arise during consolidation due to the shielding effect of a canister, the geometry of a specimen, and the density and temperature gradients within a specimen. This led to a series of mechanism-based micromechanical modeling efforts (Ref 197–202). The presence of nonhydrostatic stress states necessitates the inclusion of deviatoric stresses in the constitutive laws governing consolidation leading to the development of PROSIM, a general-purpose finite element program (Ref 191, 203, 204), and other computer programs (Ref 205) capable of analyzing deformation due to time-independent plasticity (plastic yielding) and time-dependent plasticity (power-law creep and diffusion creep). Bhagat and Rajesh (Ref 206) studied the consolidation of aluminum particles using Ashby's HIP map program. Based on the HIP map predictions, they found that the fine aluminum particles can be fully densified at an unrealistic low temperature by hot pressing (Fig. 20). This suggests that the constitutive relationships used in the HIP map program are not appropriate for fine particles (<1 μm).

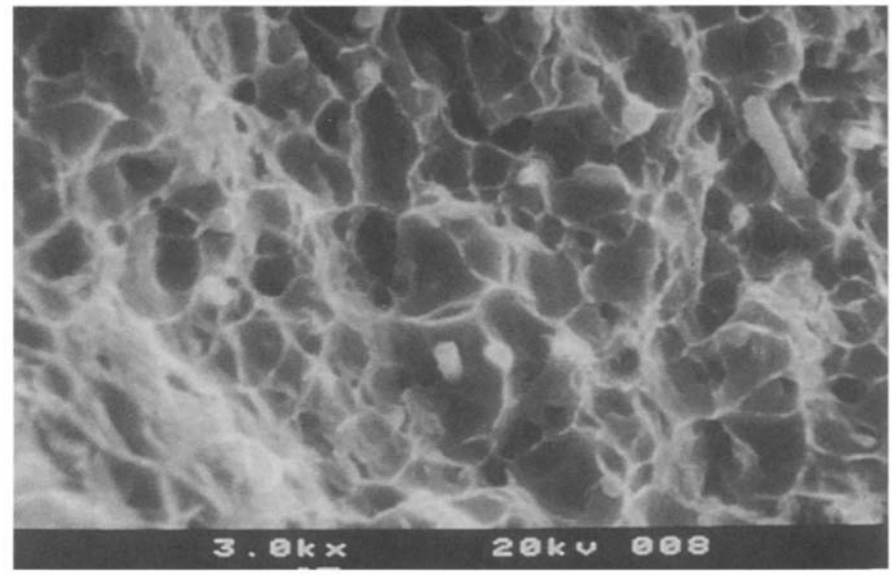

Fig. 17 Scanning electron fractograph of 6061/SiC/20$_w$ creep tested at 561 K under a load of 100 MPa.

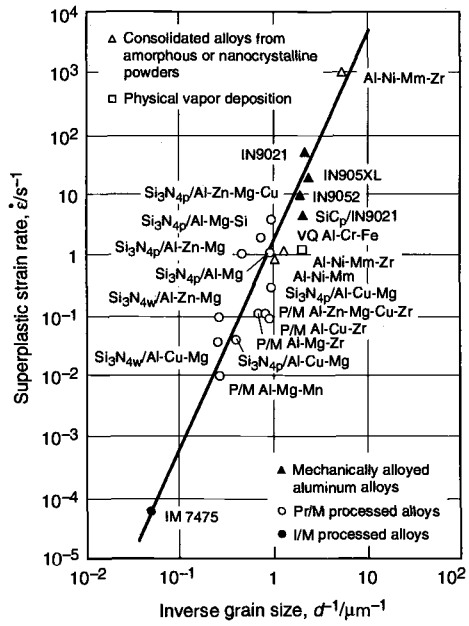

Fig. 18 The relationship between optimal superplastic strain rate and grain size for superplastic aluminum P/M alloys and composites; one I/M alloy is included for comparison. Source: Ref 187

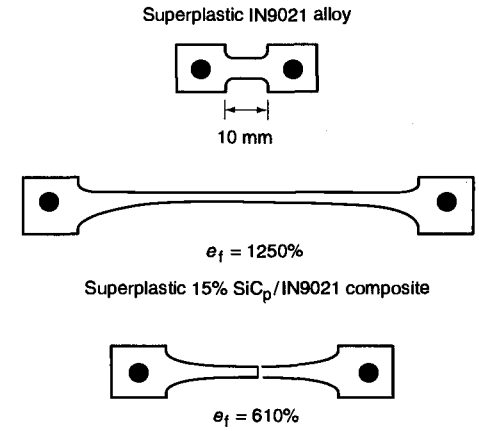

Fig. 19 Mechanically alloyed and processed samples deformed to fracture at their optimal superplastic conditions. Source: Ref 186

Machining and Joining

During conventional machining, the ceramic reinforcements dull the cutting tools, thereby reducing the machinability of the composites. The use of expensive diamond or cubic boron nitride cutting tools is not practical from cost consideration. Noncontact machining techniques such as laser processing (Ref 32) and abrasive waterjet cutting (Ref 33) appear attractive for machining these materials. Laser cutting of the SiC-whisker-reinforced aluminum composites is hampered by the formation of aluminum carbide as reported by Meinert and coworkers (Ref 207–212). They observed an aluminum carbide reaction layer on the cut surface of the composites. In addition, a significant amount of dross containing aluminum carbide remained attached to the bottom of the cut. This may be due to the

Table 11 Superplastic properties of P/M aluminum alloys and composites

Material	Grain size, μm	Solidus, °C	Test temperature, °C	Strain rate, s^{-1}	Stress, MPa	*m* value	Elongation, %
IN9021	...	495	475	1	30	...	300
IN9021	...	495	475	2	30	...	500
IN9021	0.5	495	550	50	22	0.5	1250
IN9021/SiC_p	...	495	550	5	5	0.5	600
IN9021/SiC_p	...	495	550	10	7	...	500
IN9052	0.5	580	590	10	18	0.6	330
IN905XL	...	...	550	20	5	...	200
IN905XL	0.4	...	575	20	12	0.6	190
2014/$SiC/15_p$	...	...	480	0.0004	...	0.4	395
2014/TiC	...	507	545	0.2	15	...	250
2024/$SiC/10_p$	...	...	515	0.0005	5	0.4	685
2024/$SiC/20_w$	...	...	100 ↔ 450(a)	0.0005	15	1.0	300
2124Al-0.6 wt% Zr	...	502	475	0.3	34.5	...	500
2124/$SiC/20_w$	...	502	525	0.3	10	0.33	300
2124/Si_3N_{4w}	...	502	525	0.2	10	...	250
6061/AlN	...	582	600	0.5	10	...	350
6061/SiC_w	...	582	550	0.2	6.5	...	300
6061/$SiC/20_w$	...	582	100 ↔ 450(a)	0.00001	7	1.0	1400
6061/Si_3N_4	...	582	545	0.5	20	...	450
7064/Si_3N_4	...	525	525	0.2	15	...	250
7075/$SiC/27_w$ (wt%)	...	<538	500	0.2	40	...	...
7475Al-0.9 wt% Zr	...	<538	520	0.3	13	...	900
7475Al-0.7 wt% Zr	...	<538	520	0.05	5	...	900
7475/$SiC/15_p$	...	...	515	0.0002	...	0.38	442
7475/$SiC/15_w$	...	...	520	0.0002	7	>0.5	350
Al-3.2Li-1Mg-0.3Cu-0.18Zr	...	562	570	0.1	6	...	250
Al-Ni-Mm(b)	1.0	624	612	1	15	0.5	650
Al-Ni-Mm-Zr(b)	0.8	625	600	1	15	0.5	650
RS Al-Cr-Fe	0.5	623	625	1	20	0.5	505
Al-Cu-Zr	1.6	...	500	0.01	8	0.3	600
Al-Mg-Cr	3.4	...	575	0.01	3	0.5	510
Al-Mg-Zr	1.1	...	500	0.1	21	0.3	570
Al-Zn-Mg-Cu-Zr	1.2	...	515	0.07	8	0.3	1060
Al-Mg-Mn	3.5	572	575	0.003	0.7	0.5	660
Al-Cu-Mg/Si_3N_{4p} (1 μm)	2.0	580	500	0.1	5	0.3	640
Al-Mg/Si_3N_{4p} (1 μm)	1.0	593	555	1	6	0.3	700
Al-Mg-Si/Si_3N_{4p} (0.2 μm)	1.3	582	560	2	5	0.3	620
Al-Mg-Si/Si_3N_{4p} (0.5 μm)	1.9	585	560	1	6	0.3	350
Al-Mg-Si/Si_3N_{4p} (1 μm)	3.0	580	545	0.1	5	0.3	450
Al-Cu-Mg/Si_3N_{4w}	3.3	585	560	0.1	11	0.3	480

(a) Thermal cycling. (b) Mm, mischmetal. Source: Ref 186, 188

potential reaction between the molten aluminum and the SiC whiskers, forming a highly viscous mixture of aluminum carbide and silicon. The assist gas moves the mixture toward the bottom of the cut, but is unable to expel it completely, due to its high viscosity. This results in a thin layer of aluminum carbide on the cut surface and a buildup of aluminum carbide dross at the bottom of the cut. The amount of dross attached to the bottom of the cut can be quite significant; the average height of the dross attached to the bottom of a 2 mm thick sample of the $6061/SiC/20_w$ composite was 1.25 mm. Several different assist gases, power levels, and travel speeds were used in an attempt to minimize the dross formation. Variation of processing parameters had little effect on the cut quality. The formation of aluminum carbide appears to override the ability to obtain laser cuts with a clean surface.

The weldability of the aluminum P/M alloys and composites is limited by the residual hydrogen content and wide freezing range. The hydrogen is associated with the oxides on the surface of the metal powder. Upon melting, the adsorbed hydrogen coalesces and forms pores in the fusion zone and heat-affected zone (HAZ). Minimization of the fusion-zone porosity and retention of the base alloy microstructure in the weld zone are, therefore, the major factors precluding the application of many conventional fusion-welding techniques. These alloys require the use of autogenous electon beam and pulsed Nd:YAG (neodymium:yttrium-aluminum-garnet) laser welding, which show only occasional evidence of fusion-zone porosity (Ref 213). Ellis (Ref 214) summarizes advantages and disadvantages of various joining techniques for aluminum MMCs. Solid-state (both diffusion bonding and friction welding) methods have proved very successful in joining these materials, though geometry of components may preclude these techniques. Fusion-joining techniques are often hampered by interactions between the matrix and the reinforcement material. Laser processing, however, can offer many advantages over conventional techniques. Certain precautions are necessary prior to laser-beam welding of P/M MMCs (Ref 35, 215, 216). The composites should be thoroughly degassed by vacuum annealing to minimize porosity in the weld-fusion zone. In addition, weld energy input should be controlled for preventing formation of Al_4C_3 in the SiC/Al composites.

Similar to the problem encountered during laser cutting, laser welding of SiC-reinforced aluminum composites is hampered due to the following chemical reaction between liquid aluminum and solid SiC:

$$4Al(l) + 3SiC(s) \rightarrow Al_4C_3(s) + 3Si(s) \quad \text{(Eq 2)}$$

The formation of brittle aluminum carbide platelets reduces the strength of the weld. Further degradation of the weld takes place due to the dissolution of aluminum carbide in aqueous and moist environments. The formation of aluminum carbide leads to a substantial increase in the viscosity of the melt (Ref 217). The use of aluminum alloys containing relatively high amounts of silicon is one of the most commonly used methods for eliminating the formation of aluminum carbide during molten-metal fabrication techniques. Because the formation of aluminum carbide is inhibited by the high silicon content and a relatively low melt superheat, the fusion joining of these materials is possible if the weld pool temperature is kept below that at which aluminum carbide begins to form (Ref 218). In addition to the chemical reactions, several other factors may affect the quality of the weld. For example, the reinforcement materials generally do not melt or dissolve and may segregate in the weld during the laser processing. Another com-

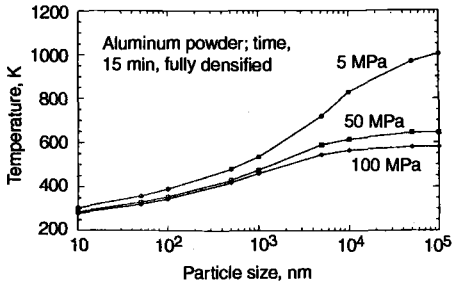

Fig. 20 Predicted temperatures according to Ashby's HIP map program for fully densifying aluminum powders by hot pressing. The plots represent 24 runs of HIP map considering eight different sizes of powder over three pressures. For each run of HIP map, the powder is assumed to have one fixed particle size.

plication is the increased viscosity of the molten pool due to the presence of the reinforcement. This can lead to a sluggish weld pool and incomplete joining.

Meinert and coworkers (Ref 207–212) used a commercially available P/M wrought 6061/$SiC/20_w$ composite (Advanced Composite Materials Corporation, Greer, SC) to study the feasibility of laser processing. A Coherent General EFA 51, 1.5 kW, enhanced fast axial flow, CO_2 gas laser, with continuous wave (CW) and pulsed TEM_{00} mode capability was used during the investigation. A focal arrangement utilizing a 6.35 mm lens produced a focused spot size of 120 μm at an output wavelength of 10.6 μm, in the infrared range. Shielding or assist gas was provided coaxial to the beam, and a computer-controlled micropositioning system was employed to manipulate the test specimens during the laser processing. The assist gas discharges the molten metal from the cut, in the case of laser cutting. In contrast, the molten metal solidifies under an inert shielding gas, in the case of laser-beam welding. The shielding gas prevents the formation of unwanted reactions and gas absorption.

The amount of laser energy absorbed by the material is one factor that determines the effectiveness of the laser processing. In general, a high absorptivity improves the processing efficiency, thereby allowing deeper penetration and faster processing speeds. Aluminum has a relatively high reflectivity, which decreases its ability to effectively absorb, or couple with the laser beam. The reinforcement materials such as aluminum oxide and SiC absorb much more energy at 10.6 μm wavelength. Initial experiments revealed that energy absorbed by the composite materials was greater than the unreinforced aluminum. The improved energy absorption is attributed to the change in reflectivity of the bulk material by the addition of the reinforcement. There appears to be a correlation between the emissivity of the material and the effectiveness of laser processing. As mentioned before, the silicon addition has been successfully used to allow the fusion joining of SiC reinforced aluminum composites (Ref 218). Suppression of the formation of aluminum carbide, however, can be achieved by additions of titanium and zirconium,

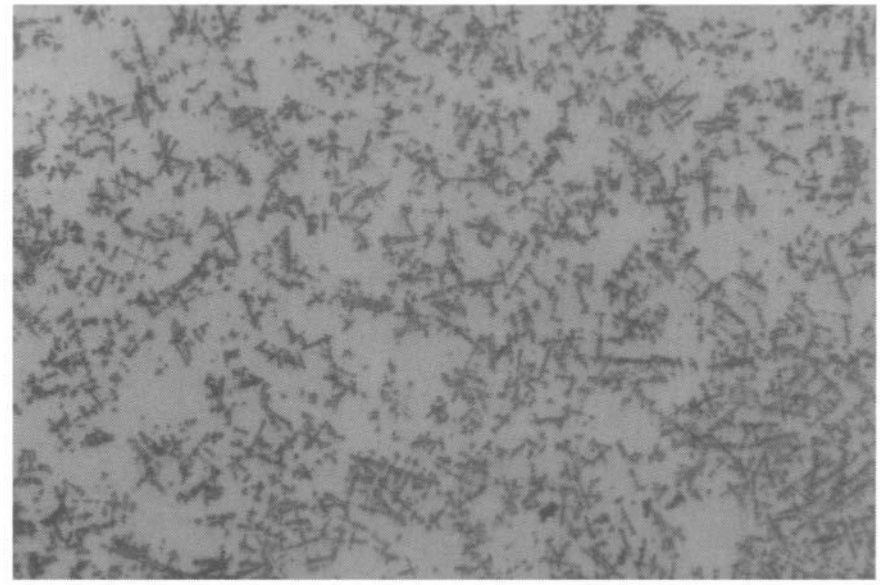

Fig. 21 Micrograph of a laser-welded $6061/SiC/20_w$ composite using titanium additions. Fine dendritic structures of TiC is evenly dispersed throughout the fusion zone.

which are strong carbide formers. Titanium carbide and zirconium carbide are also chemically stable compounds and are not subject to dissolution in water. Meinert and coworkers (Ref 207–212) laser welded $6061/SiC/20_w$ composite using commercially pure titanium additions that effectively suppressed the formation of aluminum carbide. Figure 21 shows very fine dendritic structures of TiC (1 to 5 μm) as confirmed by the electron microprobe analysis. The dendrites are evenly dispersed throughout the fusion zone. The analysis of the welds made with zirconium additions showed similar results.

Applications Outlook

In spite of a worldwide interest in developing the high-performance aluminum P/M alloys and composites, these materials have found only limited applications. With a few exceptions such as the spray-formed (Osprey) aluminum-silicon alloys for automotive parts, large-scale commercial use of the aluminum P/M alloys and composites currently does not exist. However, the outlook for potential applications of these materials in aerospace, automotive, business machines, power tools, appliances, and ordnance industries appears very bright. A few examples include:

- *Aerospace components*: Lightweight P/M aluminum alloys are attractive for major airframe primary-load-carrying structural members (Ref 219). The dispersion-strengthened aluminum-iron alloys are expected to replace conventional high-strength alloys and titanium alloys used in the manufacture of selected aerospace components such as fan and compressor cases, stiffeners, vanes and blades in gas turbine engines, fins, winglets, and rocket motor cases in missiles, and helicopter rotors. High-strength P/M 7090 is used for landing-gear assemblies (link, door actuators) (Ref 1). A high-stiffness SiC_p-reinforced 6092 Al composite has been fabricated into a ventral fin for F-16 jet fighter; the composite provides stiffness 50% higher than monolithic aluminum. The composite is expected to provide more than twice the expected life of the original fins (Ref 220). A module door for aircraft was fabricated by superplastic forming of $8090/SiC/17_p$ (Ref 120).
- *Automotive parts*: Due to their light weight, high stiffness, and wear resistance, the P/M aluminum-silicon alloys are attractive for automotive parts such as shock absorber, piston, drive shaft, brake rotor disk, engine cylinder block, autobody structures, chassis components, compressor vanes, connecting rod, and sensor housing. Ishijima et al. (Ref 121) developed forged P/M aluminum-silicon alloys for connecting rods for general-purpose engines. The fabricated connecting rods are found to be more than 30% lighter and thinner in comparison with conventional die-cast rods. Near-net shape compressor parts were fabricated by Takeda and Hayashi (Ref 122) using Al-AlN and Al-AlN-SiC composites by reaction sintering of rapidly solidified aluminum alloy/composite powder. The fabricated parts showed improved wear resistance.
- *Business machines:* Drive-belt pulleys, hubs, end caps, connecting collars, and gears
- *Appliances*: Sewing machine parts and thermostat control gears
- *Electrical and electronic applications*: Heat-sinks, substrate/housing for microelectronics package, and spacers on structural electric transmission towers
- *Ordnance*: Rifle receiver forging, mortar and artillery projectile fuses, cartridge cases, artillery shells, and rocket warheads

REFERENCES

1. *Powder Metallurgy*, Vol 7, *Metals Handbook*, 9th ed., American Society for Metals, 1984
2. H. Buhl, Ed., *Advanced Aerospace Materials*, Springer-Verlag, 1992
3. Y. Murakami, Aluminum-Based Alloys, *Materials Science and Technology*, R.W. Cahn, P. Haasen, and E.J. Kramer, Ed., Vol 8, 1996, p 213–276
4. E. Nembach, *Particle Strengthening of Metals and Alloys*, John Wiley & Sons, 1997
5. J.-W. Kim and W.M. Griffith, Ed., *Dispersion Strengthened Aluminum Alloys*, TMS, 1988
6. E.W. Lee and N.J. Kim, Ed., *Light Weight Alloys for Aerospace Applications*, TMS, 1991
7. S.S. Brenner, *J. Appl. Phys.*, Vol 33, 1962, p 33
8. S.S. Brenner, *J. Met.*, Vol 14 (No. 11), 1962, p 808
9. W.H. Sutton and J. Chorn, *Met. Eng. Q.*, Vol 3 (No. 1), 1963, p 44
10. W.H. Sutton, Whisker Composite Materials—A Prospectus for the Aerospace Designer, *Astronaut. Aeronaut.*, Aug 1966, p 46
11. A.P. Divecha, P. Lare, and H. Hahn, "Silicon Carbide Whisker Metal Matrix Composites," AFML-Tr-69-7, May 1969
12. I.B. Cutler, "Production of Silicon Carbide from Rice Hulls," U.S. Patent No. 3,754,076, Aug 1973
13. D.L. McDaniels, *Metall. Trans. A*, Vol 16, 1985, p 1105
14. R.J. Arsenault, *Mater. Sci. Eng.*, Vol 64, 1984, p 171
15. C.R. Crow, R.A. Gray, and D.F. Hasson, *Proc. of ICCM5*, W.C. Harrigan, Jr., J. Strife, and A.K. Dhingra, Ed., AIME, 1985, p 843
16. A.P. Divecha, S.G. Fishman, and S.D. Karmarkar, *J. Met.*, Vol 9 (No. 12), 1981
17. G.H. Pigott and J. Ismael, *Proc. 5th Int. Symposium on Inhaled Particles*, W.H. Walton, Ed., Pergamon Press, 8–12 Sept 1980
18. M.F. Stanton and C. Wrench, *J. Nat. Cancer Inst.*, Vol 48 (No. 3), 1972, p 797
19. T. Imai, Y. Nishida, and Y. Tozawa, Mechanical Properties of Si_3N_4 and $K_2O{\cdot}6TiO_2$ Whisker Reinforced Aluminum P/M Composites, *Proc. Fourth Japan-U.S. Conf. on Composite Materials*, Technomic, 1988, p 109–117
20. R.B. Bhagat, The Effects of Hot Pressing Parameters on the Strength of Aluminum/Stainless Steel Composites, *Metall. Trans. A*, Vol 16, 1985, p 623–628
21. R.B. Bhagat, Growth Kinetics of Interface Intermetallic Compounds in Stainless Steel Fiber Reinforced Aluminum Matrix Composites, *Interfaces in Metal Matrix Composites*, A.K. Dhingra and S.G. Fishman, Ed., TMS, 1986, p 169–183
22. R.B. Bhagat, Low Cycle Fatigue Behavior of Aluminum/Stainless Steel Composites, *AIAA J.*, Vol 23 (No. 6), 1985, p 912–917
23. R.B. Bhagat and P. Ramakrishnan, Interfacial Interactions in Aluminum Matrix Stainless Steel Fiber Composites, *Progress in Science and Engineering of Composites*, Vol 2, T. Hayashi, K. Kawata, and S. Umekawa, Ed., ICCM-IV, Tokyo, 1982, p 1297–1305
24. R.B. Bhagat and P. Ramakrishnan, Stainless Steel Fiber Reinforced Aluminum P/M Composites, *Proc. 10th Plansee Seminar, Metallwerk, Plansee, Reutte* (Austria), Vol 1, 1981, p 385–393
25. R.B. Bhagat and P. Ramakrishnan, Fabrication of Aluminum Matrix Stainless Steel Fiber Reinforced Composites, *Proc. Fourth Biennial Seminar on Gas Turbine*, GTRE, Bangalore, India, 1979, p 425–430
26. H.J. Rack and J.W. Mullins, *High Performance Powder Aluminum Alloys II*, G. Hildeman and M. Koczak, Ed., TMS, 1986, p 155–171
27. F. Wawner, A.T. Chueng, and S. Bettadapur, "Metal Matrix, Carbon, and Ceramic Composites," Technical Conference Report No. 2357, J.D. Buckley, Ed., National Aeronautics and Space Administration, 1984, p 97–118
28. T.G. Nieh, R.A. Rainen, and D.J. Chellman, *Proc. Fifth Int. Conf. Composite Materials*, W.C. Harrigan, Jr., J. Strife, and A.K. Dhingra, Ed., TMS, 1985, p 825–842
29. P.S. Gilman, Discontinuously Reinforced Aluminum: Ready for the 1990s, *JOM*, Vol 43 (No. 8), 1991, p 7
30. M.S. Zedalis, J.D. Bryant, P.S. Gilman, and S.K. Das, High Temperature Discontinuously Reinforced Aluminum, *JOM*, Vol 43 (No. 8), Aug 1991, p 29–31
31. W.C. Harrigan, Jr., Scaling-Up Particulate Reinforced Aluminum Composites for Commercial Production, *JOM*, Vol 43 (No. 8), Aug 1991, p 32–35
32. G.P. Simpson and T. J. Culkin, Laser Cutting, *Machining*, Vol 16, *ASM Handbook*, 9th ed., ASM International, 1989, p 735–742
33. J.G. Sylvia, Abrasive Waterjet Cutting, *Machining*, Vol 16, *ASM Handbook*, 9th ed., ASM International, 1989, p 743–755
34. M.K. Jain, V.V. Bhanuprasad, S.V. Kamat, A.B. Pandey, V.K. Verma, B.V.R. Bhat, and Y.R. Mahajan, Processing, Microstructure and Properties of 2124 Al-SiCp Composites, *Int. J. Powder Metall.*, Vol 29 (No. 3), July 1993, p 267–275
35. H.J. Rack, Powder Techniques in Processing of Metal Matrix Composites, *Metal Matrix Composites: Processing and Interfaces*, R.K. Everett and R.J. Arsenault, Ed., Academic Press, 1991, p 83–101
36. H.J. Rack, P. Hood, P. Nishanen, and J.L. Cook, *Proc. Third Discontinuous Metal Matrix Workshop Group* (Santa Barbara, CA), Metal Matrix Composites Information Center, 1983
37. W.C. Harrigan, Jr., Metal Matrix Composites, *Metal Matrix Composites: Processing and Interfaces*, R.K. Everett and R.J. Arsenault, Ed., Academic Press, 1991, p 1–16
38. P.E. Hood and J.P. Pickens, "Silicon Carbide Whisker Composites," U.S. Patent No. 4463058, 31 July 1984
39. V.V. Bhanuprasad, B.V.R. Bhat, A.B. Pandey, K.S. Prasad, A.K. Kuruvilla, and Y.R. Mahajan, Effect of Processing Parameters on the Properties of Discontinuously Reinforced Al/SiC P/M Composites, *Int. J. Powder Metall.*, Vol 27 (No. 3), 1991, p 227
40. C.J. Skowronek, A. Pattnaik, and R.K. Everett, "Dispersion and Blending of SiC Whiskers in RSP Aluminum Powders," Naval Research Laboratory Memorandum Report 5750, Naval Research Laboratory, 1986
41. A.P. Divecha and S.G. Fishman, Mechanical Properties of Silicon Carbide Reinforced Aluminum, *Mechanical Behavior of Materials*, Vol 3, K.J. Miller and R.F. Smith, Ed., Pergamon Press, 1979, p 351–361
42. M.Y. Wu and O.D. Sherby, Superplasticity in a Silicon Carbide Whisker Reinforced Aluminum Alloy, *Scr. Metall.*, Vol 18, 1984, p 773–776
43. A.P. Divecha, S.G. Fishman, and S.D. Karmarkar, Silicon Carbide Reinforced Aluminum—A Formable Composite, *JOM*, Vol 33, Sept 1981, p 12–17
44. J.J. Shimizu, Kusui, A. Tanaka, and O. Iwao, Whisker Reinforced Composites Prepared from Wet Ballmilled Aluminum Powder, *Metal and Ceramic Matrix Composites: Processing, Modeling and Mechanical Behavior*, R.B. Bhagat, A.H. Clauer, P. Kumar, and A.M. Ritter, Ed., Minerals, Metals and Materials Society/AIME, 1990, p 31–38
45. J.S. Benjamin, *Metall. Trans.*, Vol 1, 1970, p 2943
46. G.H. Gessinger, *Powder Metallurgy of Superalloys*, Butterworths, 1984, p 213
47. P.S. Gilman and J.S. Benjamin, *Ann. Rev. Mater. Sci.*, Vol 13, 1983, p 279
48. R. Sundaresan and F.H. Froes, *JOM*, Vol 39 (No. 8), 1987, p 22
49. C.C. Koch, Processing of Metals and Alloys, *Materials Science and Technology—A Comprehensive Treatment*, Vol 15, R.W. Cahn, Ed., VCH, 1991, p 193
50. C. Suryanarayana and F.H. Froes, *Mater. Sci. Forum*, Vol 88–90, 1992, p 445
51. C.C. Koch, *Mater. Sci. Forum*, Vol 88–90, 1992, p 243
52. C. Suryanarayana, R. Sundaresan, and F.H. Froes, *Advances in Powder Metallurgy*, Vol 3, T.G. Gasbarre and W.F. Jandeska, Jr., Ed., Metal Powder Industries Federation, 1989, p 175
53. R. Sundaresan and F.H. Froes, *Met. Powder Rep.*, Vol 44, 1989, p 195
54. C. Suryanarayana, R. Sundaresan, and F.H. Froes, *Structural Applications of Mechanical Alloying*, F.H. Froes and J.J. deBarbadillo, Ed., ASM International, 1990, p 193
55. C. Suryanarayana and F.H. Froes, *Adv. Mater.*, Vol 5, 1993, p 96
56. A. Bose, *Advances in Particulate Materials*, Butterworth-Heinemann, 1995
57. C. Suryanarayana and F.H. Froes, *J. Mater. Res.*, Vol 5, 1990, p 1880

58. F.H. Froes, C. Suryanarayana, G.-H. Chen, A. Frefer, and G.R. Hyde, *JOM,* Vol 44 (No. 5), 1992, p 26
59. H.J. Fecht, E. Hellstern, Z. Fu, and W.L. Johnson, *Metall. Trans. A,* Vol 21, 1990, p 2333
60. A. Bhaduri, V. Gopinath, and P. Ramakrishnan, SiC Particulate Reinforced Aluminum Matrix Composites Prepared by Mechanical Alloying, *Advances in Powder Metallurgy & Particulate Materials,* Part 2, Metal Powder Industries Federation, 1996, p 3–12
61. S.K. Das, Rapidly Solidified P/M Aluminum and Magnesium Alloys—Recent Developments, *Rev. Part. Mater.,* Vol 1, 1993, p 1–40
62. C. Suryanarayana, F.H. Froes, and R.G. Rowe, *Int. Mater. Rev.,* Vol 36, 1991, p 85
63. H. Jones, *Rapid Solidification of Metals and Alloys,* Institute of Metallurgists, London, 1982
64. C. Suryanarayana and F.H. Froes, *JOM,* Vol 42 (No. 3), 1990, p 22
65. S.K. Das, R.L. Bye, and P.S. Gilman, *Mater. Sci. Eng. A,* Vol 134, 1991, p 1103
66. D.J. Skinner, R.L. Bye, D. Raybould, and A.M. Brown, *Scr. Metall.,* Vol 20, 1986, p 867
67. J. Kumpfert, G. Stanick, W. Kleinekathofer, and M. Thumann, *Structural Applications of Mechanical Alloying,* F.H. Froes and J.J. de Barbadillo, Ed., ASM International, 1990, p 163
68. E.L. Courtreight et al., *Adv. Mater. Process.,* Vol 138 (No. 5), 1990, p 71
69. H.W. Jin, C.R. Park, C.G. Park, and M.C. Kim, Mechanical Strength and Thermal Stability of Al-Mm-Ni-Fe Amorphous Alloys, *Light Weight Alloys for Aerospace Applications III,* E.W. Lee, N.J. Kim, K.V. Jata, and W.E. Frazier, Ed., TMS, 1995, p 303–310
70. A. Inoue, Y.H. Kim, and T. Masumoto, *Mater. Trans., JIM,* Vol 33, 1992, p 487
71. A. Inoue, Y. Horio, Y.H. Kim, and T. Masumoto, *Mater. Trans., JIM,* Vol 33, 1992, p 669
72. Y. He, G.M. Dougherty, G.J. Shiflet, and S.J. Poon, *Acta Metall. Mater.,* Vol 41, 1993, p 337
73. Y.J. Kim, A. Inoue, and T. Masumoto, *Mater. Trans., JIM,* Vol 32, 1991, p 559
74. A. Inoue and T. Masumoto, *Encyclopedia of Materials Science and Engineering,* Supplementary Vol 2, R.W. Cahn, Ed., Pergamon, 1990, p 660–667
75. Y. He, S.J. Poon, and G.J. Shiflet, *Science,* Vol 241, 1988, p 1640
76. Y.J. Kim, A. Inoue, and T. Masumoto, *Mater. Trans., JIM,* Vol 30, 1991, p 599
77. D.J. Chellman and T.D. Bayha, Property Behavior of High Temperature Spray Deposited Al-Cu-Mg-X Alloys, *Second Int. Conf. Spray Forming, ICSF2,* J.V. Wood, Ed., Woodhead Publishing, 1993, p 427
78. I.G. Palmer, D.J. Chellman, and J. White, Evaluation of a Spray Deposited Low Density Al-Li Alloy, *Second Int. Conf. Spray Forming, ICSF2,* J.V. Wood, Ed., Woodhead Publishing, 1993, p 385
79. H. Sano, N. Tokizane, Y. Ohkubo, and K. Sibue, Spray Formed Aluminum Alloy Components for Automotive Applications, *Second Int. Conf. Spray Forming, ICSF2,* J.V. Wood, Ed., Woodhead Publishing, 1993, p 363
80. T.D. Bayha and D.J. Chellman, Elevated Temperature Fracture Behavior of Spray Deposited 2618 Extrusions, *Advances in Powder Metallurgy & Particulate Materials,* Vol 5, Metal Powder Industries Federation, 1994, p 17
81. A.R.E. Singer, Metal Matrix Composites Made by Spray Forming, *Mater. Sci. Eng. A,* Vol 135, 1991, p 13–17
82. J.H. Tweed, J. Watling, J. Cook, J. Crook, A.D. Simpson, and I.W. Pearson, Characterization of the Uniformity and Filler Content of a Spray Formed 8090/SiC Composite, *Second Int. Conf. Spray Forming, ICSF2,* J.V. Wood, Ed., Woodhead Publishing, 1993, p 319
83. A. Lawley and D. Apelian, Spray Forming of Metal Matrix Composites, *Second Int. Conf. Spray Forming, ICSF2,* J.V. Wood, Ed., Woodhead Publishing, 1993, p 267
84. M. Gupta, J. Juarez-Islas, W.E. Frazier, F. Mohamed, and E.J. Lavernia, Microstructure, Excess Solid Solubility and Elevated-Temperature Mechanical Behavior of Spray-Atomized and Codeposited Al-Ti-SiCp, *Metall. Trans. B,* Vol 23, 1992, p 719–736
85. M. Gupta, F. Mohamed, and E.J. Lavernia, *J. Mater. Manuf. Proc.,* Vol 5, 1990, p 165–176
86. T.S. Srivatsan and E.J. Lavernia, Use of Spray Techniques to Synthesize Particulate-Reinforced Metal-Matrix Composites, *J. Mater. Sci.,* Vol 27 (No. 22), 1992, p 5965–5981
87. Y. Wu and E.J. Lavernia, Interaction Mechanisms between Ceramic Particles and Atomized Metallic Droplets, *Metall. Trans. A,* Vol 23 (No. 10), 1992, p 2923–2935
88. P.J. Ward, I.G. Elias, and H.V. Atkinson, Processing Parameters in the Spray-Forming and Subsequent Semi-Solid Forming of Hypereutectic Al/Si Based MMCs, *Second Int. Conf. Spray Forming, ICSF2,* J.V. Wood, Ed., Woodhead Publishing, 1993, p 303
89. J. White, K. Mingard, I.R. Hughes, and I.G. Palmer, Aluminum Alloys with Unique Property Combinations by Spray Casting, *Second Int. Conf. Spray Forming, ICSF2,* J.V. Wood, Ed., Woodhead Publishing, 1993, p 355
90. R.B. Bhagat and M.F. Amateau, Droplet Solidification and Microstructures Modeling for Aluminum-Lithium Alloys, *Advances in Powder Metallurgy & Particulate Materials,* Vol 7, Metal Powder Industries Federation, 1996, p 347–364
91. R.B. Bhagat, "Coarsening Kinetics of Solid Particles in the Spray-Formed (Osprey) Aluminum Alloy Preform," presented at 126th TMS Annual Meeting (Orlando), 9–13 Feb 1997
92. C.L. Buhrmaster, D.E. Clark, and H.B. Smartt, Spray Casting Aluminum and Al/SiC Composites, *JOM,* Vol 40 (No. 11), 1988, p 44–45
93. T.C. Willis, Spray Deposition Process for Metal Matrix Composites Manufacture, *Met. Mater.,* Aug 1988
94. T.C. Willis, J. White, R.M. Jordan, and I.R. Hughes, Microstructure and Properties of Al-SiC Composite Materials Produced by Spray Deposition, *Solidification Processing,* Institute of Metals, 1988, p 476–478
95. T.J. Warner et al., *ICCI II Proc.,* Case Western Reserve University (Cleveland), June 1988
96. Y. Wu and E.J. Lavernia, Spray-Atomized and Codeposited 6061 Al/SiC_p Composites, *JOM,* Vol 43 (No. 8), Aug 1991, p 16–23
97. P.A. Siemers, M.R. Jackson, R.L. Mehan, and J.R Rairden III, Production of Composite Structures by Low-Pressure Plasma Deposition, *Ceram. Eng. Sci. Proc.,* Vol 6 (No. 7–8), 1985, p 896–907
98. L. Christodoulou, P.A. Parrish, and C.R. Crowe, *High Temperature/High Performance Composites,* F.D. Lamkey, S.G. Fishman, A.G. Evans, and J.R. Strife, Ed., Vol 120, Materials Research Society, 1988, p 29
99. D.E. Larsen, M.L. Adams, S.L. Kampe, L. Christodoulou, and J.D. Bryant, Influence of Matrix Phase Morphology on Fracture Toughness in a Discontinuously Reinforced XD Titanium Aluminide Composite, *Scr. Metall.,* Vol 24, 1990, p 851–856
100. H.L. Marcus and D.L. Bourell, Solid Preform Fabrication Finds New Application, *Adv. Mater. Process.,* Vol 144 (No. 3), Sept 1993, p 28–35
101. T. Studt, Rapid Prototyping Key to Fast Development, *R&D,* May 1994, p 55–56
102. Z.A. Munir, The Synthesis and Consolidation of Powders by Self-Propagating Combustion Methods, *Rev. Part. Mater.,* Vol 1, A. Bose, R.M. German, and A. Lawley, Ed., 1993, p 41–74
103. Z.A. Munir, *Am. Ceram. Soc. Bull.,* Vol 67, 1988, p 342
104. J.B. Holt and S.D. Dunmead, *Ann. Rev. Mater. Sci.,* Vol 21, 1991, p 305
105. Z.A. Munir and J.B. Holt, *J. Mater. Sci.,* Vol 22, 1987, p 710
106. S. Zhang and Z.A. Munir, *J. Mater. Sci.,* Vol 36, 1991, p 3380
107. A. Mortensen and M.J. Koczak, The Status of Metal Matrix Composite Research and Development in Japan, *JOM,* Vol 45 (No. 3), March 1993, p 10–18
108. M. Koizumi, Recent Progress of Functionally Gradient Materials in Japan, *Ceram. Eng. Sci. Proc.,* Vol 13, 1992, p 333–346
109. F.S. Petit, High Performance/High Temperature Materials in Japan, *Sci. Bull.,* Vol 17, 1992, p 119–130
110. R. Ford, Recent Developments in Functionally Gradient Materials, *Mater. Process. Rep.,* Vol 7, 1992, p 1–6
111. M. Sunakawa, "Current Status of R&D in Japan on Materials for Space Planes," Technical Paper 91-6096, 91-5096, American Institute of Aeronautics and Astronautics, 1991
112. G.P. Yiasemides and N.J.E. Adkins, The Application of the Graded Structures Concept to

Engineering Materials, *Advances in Powder Metallurgy & Particulate Materials*, Vol 9, Metal Powder Industries Federation, 1992, p 69–80
113. K. Atarashiya, K. Kurukawa, and T. Nagai, Functionally Gradient Material of the System Ni-MgO, Ni-NiO, Ni-Si_3N_4 or Al-AlN by Pressureless Sintering, *Ceram. Eng. Sci. Proc.*, Vol 13, 1992, p 400–407
114. M.P. Thomas and J.E. King, Improvement of the Mechanical Properties of 2124Al/SiC_p MMC Plate by Optimization of the Solution Treatment, *Compos. Sci. Technol.*, Vol 56, 1996, p 1141–1149
115. B.V.R. Bhat, Y.R. Mahajan, H.M.D. Roshan, and Y.V.R.K. Prasad, Processing Maps for Hot-Working of Powder Metallurgy 1100Al-10vol% SiC-Particulate Metal-Matrix Composite, *J. Mater. Sci.*, Vol 27, 1992, p 2141–2147
116. A.L. Geiger and J.A. Walker, The Processing and Properties of Discontinuously Reinforced Aluminum Composites, *JOM*, Vol 43 (No. 8), Aug 1991, p 8–15
117. G. Staniek and F. Lehnert, Powder Metallurgy of Aluminum Alloys, *Advanced Aerospace Materials*, H. Buhl, Ed., Springer-Verlag, 1992, p 47–58
118. B. Wang, G.M. Janowski, and B.R. Patterson, Particle Cracking in P/M Processed SiC-Reinforced Aluminum Matrix Composite Materials, *Advances in Powder Metallurgy & Particulate Materials*, Vol 6, Metal Powder Industries Federation, 1993, p 161–173
119. T.J.A. Doel, M.H. Loretto, and P. Bowen, Mechanical Properties of Aluminum Based Particulate Metal Matrix Composites, *Composites*, Vol 24 (No. 3), 1993, p 270–275
120. M. Hunt, Aerospace Composites, *Mater. Eng.*, Vol 108 (No. 6), June 1991, p 27–30
121. Z. Ishijima, H. Shikata, H. Urata, and S. Kawase, Development of P/M Forged Al-Si Alloy for Connecting Rod, *Advances in Powder Metallurgy & Particulate Materials*, Part 14, Metal Powder Industries Federation, 1996, p 3–13
122. Y. Takeda and T. Hayashi, Properties of Reaction-Sintered Al-AlN and Al-AlN-SiC Composite Alloys, *Advances in Powder Metallurgy & Particulate Materials*, Part 10, Metal Powder Industries Federation, 1996, p 41–49
123. H. Li, J.B. Li, L.Z. Sun, and Z.G. Wang, Modification of the Residual Stress State in a SiC_p/6061Al Composite by Low-Temperature Treatment, *Compos. Sci. Technol.*, Vol 57, 1997, p 165–172
124. J. Cernyar, F. Yang, and A. Saxena, Fracture and Fatigue Crack Growth Behavior of SiC_w/2124Al Composite, *J. Compos. Technol. Res.*, Vol 18 (No. 1), 1996, p 30–37
125. I.J. Polmear, *Light Alloys: Metallurgy of the Light Metals*, American Society for Metals, 1982, p 76–79
126. S. Krishnamurthy, Y.W. Kim, G. Das, and F.H. Froes, *Metal and Ceramic Matrix Composites*, R.B. Bhagat, A.H. Clauer, P. Kumar, and A.M. Ritter, Ed., TMS, 1990, p 145
127. K. Komai, K. Minoshima, and H. Ryoson, Tensile and Fatigue Fracture Behavior and Water-Environment Effects in a SiC-Whisker/7075 Aluminum Composite, *Compos. Sci. Technol.*, Vol 46, 1993, p 59–66
128. A. Sakamoto, H. Hasegawa, and Y. Minoda, Mechanical Properties of SiC Whisker Reinforced Aluminum Composites, *Fifth Int. Conf. Composite Materials, ICCM-V* (San Diego), W.C. Harrigan, Jr., J. Strife, and A.K. Dhingra, Ed., 1985, p 699–707
129. H. Kashiwaya, M. Morita, K. Hagata, T. Nishimura, T. Miyamoto, and Y. Ishiwata, Mechanical Characteristics of Bolts Made of SiC Whisker Reinforced 6061 Aluminum Alloy Composite, *Composites '86: Recent Advances in Japan and the United States*, K. Kawata, S. Umekawa, and A. Kobayashi, Ed., Proc. Japan-U.S. CCM III, Tokyo, 1986, p 529–536
130. D.F. Hasson, S.M. Hoover, and C.R. Crowe, Effect of Thermal Treatment on the Mechanical and Toughness Properties of Extruded SiC with Aluminum 6061 Metal Matrix Composite, *J. Mater. Sci.*, Vol 20, 1985, p 4147–4154
131. T.G. Nieh, K. Xia, and T.G. Langdon, Mechanical Properties of Discontinuous SiC Reinforced Aluminum Composites at Elevated Temperatures, *J. Eng. Mater. Technol.*, Vol 10, 1988, p 77–82
132. C.E. da Costa, J.M. Torralba, J.M. Ruiz-Prieto, J.M. Badia, V. Amigo, and W.C. Zapata, P/M 2014 Aluminum Alloy Obtained by Mechanical Alloying, *Advances in Powder Metallurgy & Particulate Materials*, Part 2, Metal Powder Industries Federation, 1996, p 23–31
133. P. Ramakrishnan, "Novel Processing of P/M Aluminum Matrix Composites," P/M World Congress (San Francisco), June 1992
134. M. Takeyama and C.T. Liu, Effects of Grain Size and Test Temperature on Ductility and Fracture Behavior of a B-Doped Ni_3Al Alloy, *Acta Metall.*, Vol 36 (No. 5), 1988, p 1241–1249
135. K. Sampath and W.A. Baeslack III, Joining Dispersion-Strengthened, Rapidly Solidified P/M Al Alloys, *JOM*, Vol 46 (No. 7), 1994, p 41–47
136. K.A. Khor, Z.H. Yuan, and F. Boey, Processing of Submicron SiC Reinforced Al-Li Composites by Mechanical Milling, *Processing and Fabrication of Advanced Materials IV*, T.S. Srivatsan and J.J. Moore, Ed., TMS, 1996, p 499–507
137. F.H. Froes, *Mater. Edge*, Vol 5, 1988, p 19
138. A. Bhaduri, V. Gopinathan, P. Ramakrishnan, and A.P. Miodownik, *Int. Conf. Advances in Materials and Process Processes*, ASM International, India Chapter, 16–19 Feb 1992
139. I.A. Ibrahim, F.A. Mohamed, and E.J. Lavernia, *Advanced Aluminum and Magnesium Alloys*, T. Khan and G. Effenberg, Ed., ASM International, 1990, p 745–754
140. J.L. Estrada and J. Duszczyk, Sintering of High Temperature Resistant P/M Aluminum Alloys, *Advances in Powder Metallurgy & Particulate Materials*, Part 11, Metal Powder Industries Federation, 1996, p 129–141
141. R.H. Dauskardt, R.O. Ritchie, and B.N. Cox, Fatigue of Advanced Materials: Part I, *Adv. Mater. Process.*, Vol 144 (No. 1), July 1993, p 26–31
142. J.K. Shang and G. Liu, *Role of Composite Interface in Fatigue Crack Growth, Control of Interfaces in Metal and Ceramic Composites*, R.Y. Lin and S.G. Fishman, Ed., Minerals, Metals and Materials Society/AIME, 1993, p 187–196
143. D.L. Davidson, Fatigue and Fracture Toughness of Aluminum Alloys Reinforced with SiC and Alumina Particles, *Composites*, Vol 24 (No. 3), 1993, p 248–255
144. S. Kumai, J.E. King, and J.F. Knott, Short and Long Fatigue Crack Growth in a SiC Reinforced Aluminum Alloy, *Fatigue Fract. Eng. Mater. Struct.*, Vol 13, 1990, p 511–524
145. T.J. Downes, D.M. Knowles, and J.E. King, The Effect of Particle Size on Fatigue Crack Growth in an Aluminum Based Metal Matrix Composite, *Fatigue of Advanced Materials*, R.O. Ritchie, R.H. Dauskardt, and B.N. Cox, Ed., p 395–407
146. R.M. McMeeking, Finite Deformation Analysis of Crack-Tip Opening in Elastic-Plastic Materials and Implications for Fracture, *J. Mech. Phys. Solids*, Vol 25, 1977, p 357–381
147. T.C. Willis, Spray Deposition Process for Metal Matrix Composites Manufacture, *Met. Mater.*, Vol 4, 1988, p 485–488
148. M.T. Narasimhan, R.B. Bhagat, and R.N. Pangborn, Thermomechanical Fatigue Performance of Silicon Carbide Whisker Reinforced Aluminum Composite, 1998
149. A.B. Gurcan and T.N. Baker, Wear Behavior of AA6061 Aluminum Alloy and Its Composites, *Wear*, Vol 188, 1995, p 185–191
150. A.P. Sannino and H.J. Rack, Dry Sliding Wear of Discontinuously Reinforced Aluminum Composites: Review and Discussion, *Wear*, Vol 189, 1995, p 1–19
151. C. Jin, K.-M. Cho, and I. Park, Wear Properties of High Temperature Al Alloys, *Light Weight Alloys for Aerospace Applications III*, E.W. Lee, N.J. Kim, K.V. Jata, and W.E. Frazier, Ed., TMS, 1995, p 43–55
152. D. Bialo and J. Duszczyk, Wear of Aluminum Matrix Composites Processed by Liquid Phase Sintering and Hot Extrusion, *Advances in Powder Metallurgy & Particulate Materials*, Part 16, Metal Powder Industries Federation, 1996, p 17–22
153. A. Wang and H.J. Rack, The Effect of Aging on the Abrasion Behavior of SiC_w/2124 Al Metal Matrix Composites, *Advanced Metal and Ceramic Matrix Composites: Processing, Modeling and Mechanical Behavior*, R.B. Bhagat, A.H. Clauer, P. Kumar, and A.M. Ritter, Ed., TMS, 1990, p 487–498
154. T.J. Downes and J.E. King, The Effect of Microstructure on the Fracture Toughness of a

Metal Matrix Composite, *Composites,* Vol 24 (No. 3), 1993, p 276–281
155. R.B. Bhagat and M.B. House, Elevated Temperature Mechanical Properties of Silicon Carbide Whisker Reinforced Aluminum Matrix Composites, *Mater. Sci. Eng. A,* Vol 144, 1991, p 319–326
156. R.B. Bhagat, M.B. House, and M.F. Amateau, Aging Characteristics and Mechanical Properties of Silicon Carbide Whisker Reinforced Aluminum Matrix Composites, *Proc. 1990 Powder Metallurgy Conf.* (Pittsburgh), May 1990
157. M.B. House, K.C. Meinert, and R.B. Bhagat, The Aging Response and Creep of DRA Composites, *JOM,* Aug 1991, p 24–28
158. R.B. Bhagat, M.F. Amateau, M. House, K.C. Meinert, and P. Nisson, Elevated Temperature Strength, Aging Response and Creep of Aluminum Matrix Composites, *J. Compos. Mater.,* Vol 26 (No. 11), 1992, p 1578–1593
159. R.B. Bhagat, M.F. Amateau, M.B. House, K.C. Meinert, and P. Nisson, Elevated Temperature Strength, Aging Response and Creep of Aluminum Matrix Composites, *Proc. Eighth Int. Conf. Composite Materials, ICCM VIII* (Honolulu), S.W. Tsai and G.S. Springer, Ed., SAMPE, Covina, CA, 15–19 July 1991, p 20C2–20C13
160. T. Christman and S. Suresh, Microstructural Development in and Aluminum Alloy-SiC Whisker Composite, *Acta Metall.,* Vol 36 (No. 7), 1988, p 1691–1704
161. M.J. Birt and W.S. Johnson, Characterization of the Tensile and Microstructural Properties of an Aluminum Metal Matrix Composite, *Fundamental Relationships between Microstructure and Mechanical Properties of Metal Matrix Composites,* P.K. Liaw and M.H. Gungor, Ed., TMS, 1990, p 71–88
162. T.G. Nieh and R.F. Karlak, Aging Characteristics of B4C-Reinforced 6061-Aluminum, *Scr. Metall.,* Vol 18, 1984, p 25–28
163. K.H. Oh, H.I. Lee, T.S. Kim, and T.H. Kim, Effect of SiC Whisker Reinforcement on the Precipitation Behaviors/Tensile Properties of Al-Cu-(Mg,Li) Alloys, *Fundamental Relationships between Microstructure and Mechanical Properties of Metal Matrix Composites,* P.K. Liaw and M.H. Gungor, Ed., TMS, 1990, p 115–126
164. S. Dionne, M.R. Krisknadev, and R. Bouchard, Effects of Heat Treatment on the Microstructure and Tensile Properties of A P/M SiC Particulate/7091 Al MMC, *Advanced Metal and Ceramic Matrix Composites: Processing, Modeling and Mechanical Behavior,* R.B. Bhagat, A.H. Clauer, P. Kumar, and A.M. Ritter, Ed., TMS, 1990, p 243–252
165. S.R. Nutt, Interfaces and Failure Mechanisms in Al-SiC Composites, *Interfaces in Metal-Matrix Composites,* A.K. Dhingra and S.G. Fishman, Ed., TMS, 1986, p 157–167
166. F.R.N. Nabarro and H.L. de Villiers, *The Physics of Creep,* Taylor & Francis, 1995
167. R.S. Mishra and A.K. Mukherjee, Creep Behavior of Rapidly Solidified and Processed Aluminum Alloys, *Light Weight Alloys for Aerospace Applications III,* E.W. Lee, N.J. Kim, K.V. Jata, and W.E. Frazier, Ed., TMS, 1995, p 319–332
168. R.S. Mishra, A.G. Paradkar, and K.N. Rao, Steady State Creep Behavior of a Rapidly Solidified and Further Processed Al-5 wt% Ti Alloy, *Acta Metall. Mater.,* Vol 41, 1993, p 2243–2251
169. M.K. Premkumar, M.J. Koczak, and A. Lawley, Elevated Temperature Mechanical Behavior of P/M Dispersion Strengthened Al-Fe-Ni Alloys, *High Strength Powder Metallurgy Aluminum Alloys II,* G. Hildeman and M.J. Koczak, Ed., TMS, 1986, p 265–284
170. M.K. Premkumar, A. Lawley, and M.J. Koczak, Mechanical Behavior of Powder Metallurgy Al-Fe-Ni Alloys, *Mater. Sci. Eng. A,* Vol 174, 1994, p 127–139
171. D. Legzdina and T.A. Parthasarathy, Deformation Mechanisms of a Rapidly Solidified Al-8.8Fe-3.7Ce Alloy, *Metall. Trans. A,* Vol 18, 1987, p 1713–1719
172. D. Legzdina and T.A. Parthasarathy, Effect of Cerium Content on the Deformation Behavior of Rapidly Solidified Al-Fe-Ce Alloys, *Metall. Trans. A,* Vol 21, 1990, p 2155–2158
173. G.M. Pharr et al., High Temperature Creep Deformation of a Rapidly Solidified Al-Fe-V-Si Alloy, *Dispersion Strengthened Aluminum Alloys,* Y.-W. Kim and W.M. Griffith, Ed., TMS, 1988, p 309–322
174. S.C. Khatri et al., Creep and Microstructural Stability of Dispersion Strengthened Al-Fe-V-Si-Er Alloy, *Mater. Sci. Eng. A,* Vol 167, 1993, p 11–21
175. R.S. Mishra, H. Jones, and G.W. Greenwood, Creep of a Rapidly Solidified and Further Processed Al-Cr-Zr Alloy, *Int. J. Rapid Solidif.,* Vol 5, 1990, p 149–162
176. Y.C. Chen, M.E. Fine, and J.R. Weertman, Microstructural Evolution and Mechanical Properties of Rapidly Solidified Al-Zr-V Alloys at High Temperatures, *Acta Metall. Mater.,* Vol 38, 1990, p 771–780
177. W.W. Park and H. Jones, The Creep Behavior of Rapidly Solidified Al-Zr-V Alloys at Low Stresses, *Mater. Sci. Eng. A,* Vol 134, 1991, p 1229–1233
178. J.E. Benci and W.E. Frazier, Evaluation of a New Aluminum Alloy for 700 °F Aerospace Applications, *Light Weight Alloys for Aerospace Applications,* E.W. Lee and N.J. Kim, Ed., TMS, 1991, p 231–245
179. T.G. Nieh, Creep Rupture of a Silicon Carbide Reinforced Aluminum Composite, *Metall. Trans. A,* Vol 15, Jan 1984, p 139–145
180. V.C. Nardone and J.R. Strife, Analysis of the Creep Behavior of Silicon Carbide Whisker Reinforced 2124 Al (T4), *Metall. Trans. A,* Vol 18, 1987, p 109–114
181. T. Morimoto, T. Yamaoka, H. Lilholt, and M. Taya, Second Stage Creep of SiC Whisker/6061 Aluminum Composite at 573 K, *J. Eng. Mater. Technol.,* Vol 110, April 1988, p 70–76
182. E.P. Barth, J.T. Morton, and J.K. Tien, Threshold for Creep Resistance in a Silicon Carbide Reinforced Aluminum Alloy, *Fundamental Relationships between Microstructures and Mechanical Properties of Metal Matrix Composites,* TMS, 1990
183. R.E. Smallman, *Modern Physical Metallurgy,* 4th ed., Butterworth, 1985
184. W.A. Spitzig, C.L. Trybus, and J.D. Verhoeven, Deformation-Processed Metal/Metal Composites, *Metal Matrix Composites: Processing and Interfaces,* R.K. Everett and R.J. Arsenault, Ed., Academic Press, 1991, p 151–179
185. A. Jokinen and B. Wiik, "Formability of Aluminum Alloy Matrix Composites," P/M World Congress (San Francisco), June 1992
186. K. Higashi, M. Mabuchi, and T.G. Langdon, High-Strain-Rate Superplasticity in Metallic Materials and the Potential for Ceramic Materials, *ISIJ Int.,* Vol 36 (No. 12), 1996, p 1423–1438
187. T.G. Nieh, J. Wadsworth, and O.D. Sherby, *Superplasticity in Metals and Ceramics,* Cambridge University Press, 1997
188. T.K. Ha and Y.W. Chang, High Temperature Deformation Behavior of 8090 Al-Li Alloy, *Light Weight Alloys for Aerospace Applications III,* E.W. Lee, N.J. Kim, K.V. Jata, and W.E. Frazier, Ed., TMS, 1995, p 281–289
189. M. Mabuchi and T. Imai, Superplasticity of Si_3N_4 Whisker Reinforced 6061 Aluminum at High Strain Rate, *J. Mater. Sci. Lett.,* Vol 9, 1990, p 761–762
190. T. Imai and M. Mabuchi, Superplasticity in Silicon Nitride Whisker Reinforced 2124 Aluminum Alloy Composite, *J. Jpn. Inst. Light Met.,* Vol 39, 1989, p 831–835
191. T.F. Zahrah and L. Christodoulou, Modeling and Design of P/M Consolidation Processes, *Advances in Powder Metallurgy & Particulate Materials,* Vol 3, Metal Powder Industries Federation, 1993, p 77–83
192. M.G. McKimpson and K.L. Paxton, Effect of Reinforcement Distribution on the Densification Behavior of Metal-Ceramic Composites at Isostatic Pressures Greater than 200 MPa, *Advances in Powder Metallurgy & Particulate Materials,* Vol 3, Metal Powder Industries Federation, 1993, p 215–228
193. A.S. Helle, K.E. Easterling, and M.F. Ashby, *Acta Metall.,* 1985
194. M.F. Ashby, *HIP 6.0 Background Reading,* Engineering Dept., Cambridge University, 1990
195. E. Arzt, *Acta Metall.,* Vol 30, 1982, p 1883
196. E. Arzt, M.F. Ashby, and K.E. Easterling, *Metall Trans. A,* Vol 14, 1983, p 211
197. L.T. Kuhn and R.M. McMeeking, *Int. J. Mech. Sci.,* Vol 34, 1991, p 563
198. N.A. Fleck, L.T. Kuhn, and R.M. McMeeking, *J. Mech. Phys. Solids,* Vol 40, 1991, p 1139
199. R.M. McMeeking and L.T. Kuhn, *Acta Metall. Mater.,* Vol 40, 1991, p 961

200. A.L. Gurson, *Int. J. Mech. Sci.*, Vol 14, 1977, p 215
201. P. Sofornis and R.M. McMeeking, *J. Appl. Mech.*, Vol 59, 1992, p 888
202. H. Riedel, *Ceramic Powder Science III*, G.L. Messing, Ed., 1990, p 619
203. W.P. Li, M.F. Ashby, and K.E. Easterling, *Acta Metall.*, Vol 35 (No. 12), 1987
204. T.F. Zahrah, C.J. Coe, and F.H. Charron, The Role of Process Models in Intelligent Hot Isostatic Pressing of Powder Materials, *Proc. Symposium on Applications of Mechanics and Materials Models to Design and Processing*, TMS, 4–5 March 1992
205. J. Xu and R. McMeeking, Modeling Powder Consolidation and the Formation of Composite Materials, *Advances in Powder Metallurgy & Particulate Materials*, Vol 3, Metal Powder Industries Federation, 1993, p 201–214
206. R.B. Bhagat and G. Rajesh, 1998 (unpublished work)
207. K.C. Meinert, Jr., R.B. Bhagat, and R. Martukanitz, "Laser Processing of Discontinuously Reinforced Aluminum Composites," Technical Report, File No. TR 94-001, Applied Research Laboratory, Pennsylvania State University, University Park, PA, 1994
208. R.B. Bhagat, R.P. Martukanitz, and K.C. Meinert, Jr., Laser Processing of Discontinuously Reinforced Aluminum Composites, *ARL Review*, 1993
209. K.C. Meinert, Jr., R.P. Martukanitz, and R.B. Bhagat, Laser Processing of Discontinuously Reinforced Aluminum Composites, *Proc. American Society for Composites Seventh Technical Conf. Composite Materials*, The Pennsylvania State University, University Park, PA, 13–15 Oct 1992, p 168–177
210. K.C. Meinert, Jr., R.P. Martukanitz, R.B. Bhagat, and J. Eckert, "Laser Welding of SiC Reinforced Aluminum Composites," presented at Aeromat '92 (Anaheim, CA), 18–21 May 1992
211. R.P. Martukanitz and R.B. Bhagat, Laser Processing of Discontinuously Reinforced Aluminum Matrix Composites, *The Metal Science of Joining*, M.J. Cieslak, J.H. Perepezko, S. Kang, and M.E. Glicksman, Ed., TMS, 1992, p 241–248
212. K.C. Meinert, Jr., R.P. Martukanitz, and R.B. Bhagat, Laser Cutting and Welding of Discontinuously Reinforced Aluminum Composites, *TMS Conf. Proceedings* (Denver), Spring 93
213. K. Sampath and W.A. Baeslack III, Weldability of a RS-PM Al-8Fe-2Mo Alloy, *Weld. J.*, Vol 72 (No. 8), 1993, p 416s–427s
214. M.B.D. Ellis, Joining of Aluminum Based Metal Matrix Composites, *Int. Mater. Rev.*, Vol 41 (No. 2), 1996, p 41–58
215. J. Ahern, C. Cook, and S.G. Fishman, *Met. Constr.*, Vol 14, 1982, p 192
216. T.S. Luhman, R.L. Williams, and K.B. Das, "Development of Joint and Joint Techniques for Metal Matrix Composites," AMMRC-TR 84-35, Army Laboratory, Boston, Aug 1984
217. D.M. Schuster, M.D. Skibo, and W.R. Hoover, Production and Semi-Fabrication of an Aluminum Composite Material: Extrusion and Casting Considerations, *Light Metal Age*, Feb 1989, p 15–19
218. *Arc Welding Guidelines*, Duralcan, 1991
219. J.T. Staley, J. Liu, and W.H. Hunt, Jr., Aluminum Alloys for Aerostructures, *Adv. Mater. Process.*, Oct 1997, p 17–20
220. M.V.D. Berg, Aluminum Composite Doubles Lifetime of F-16 Ventral Fin, *Adv. Mater. Process*, Oct 1996, p 7